Radiative Transfer in the Atmosphere for Correction of Ocean Color Remote Sensors

by

Howard R. Gordon
Department of Physics
University of Miami
Coral Gables, FL 33124

Presented at the International Space Year '92 *Productivity of the Global Ocean (PGO)* Activity: Working Group Meeting & Workshop on *OCEAN COLOR: THEORY AND APPLICATIONS IN A DECADE OF CZCS EXPERIENCE*, JRC CEC, Ispra, Italy, October 21–25, 1991.

Acknowledgement

The author is grateful to M. Wang for carrying out the LOWTRAN-7 simulations, and to the National Aeronautics and Space Administration for providing support under Grant NAGW-273.

Attachment 1.16

Introduction

Following the work of Clarke, Ewing, and Lorenzen[1] showing that the chlorophyll concentration in the surface waters of the ocean could be deduced from aircraft measurements of the spectrum of upwelling light from the sea — the "ocean color" — NASA launched the Coastal Zone Color Scanner (CZCS) on Nimbus-7 in late 1978.[2,3] The CZCS was a proof-of-concept mission with the goal of measuring ocean color from space. It was a scanning radiometer that had four bands in the visible at 443, 520, 550, and 670 nm with bandwidths of 20 nm, one band in the near infrared (NIR) at 750 nm with a band width of 100 nm, and a thermal infrared band (10.5 to 12.5 μm) to measure sea surface temperature. The four visible bands possessed high radiometric sensitivity (well over an order of magnitude higher than other sensors designed for earth resources, e.g., the MSS on the Landsat series) and were specifically designed for ocean color. Further technical details concerning CZCS are given in the Appendix. The CZCS experience demonstrated the feasibility of the measurement of plankton pigments, and possibly even productivity,[4,5] on a *global* scale. This feasibility rests squarely on two observations: (1) there exists a more or less universal relationship between the color of the ocean and the plankton pigment concentration for most open ocean waters; and (2) it is possible to develop algorithms to remove the interfering effects of scattering in the atmosphere. In this paper we will review the atmospheric effects associated with CZCS.

The paper is structured in the following way. First, the basic concepts of radiometry that are required to understand radiative transfer are presented. Second, the relevant optical properties of the atmosphere are reviewed in detail. Next, the radiative transfer equation is introduced, a method of solution is described, and a first order solution derived for a scattering atmosphere. This solution is then applied to the development of the CZCS atmospheric correction algorithm. The shortcomings of the algorithm are then discussed along with the modifications that improve its performance with CZCS. Finally, I provide some indication of the modifications to the correction algorithm that will be required for the new, more sensitive, ocean color instruments, e.g., SeaWiFS to be launched in late 1993.

Atmospheric Optical Properties

Radiance

Light of wavelength λ (SI unit: nm) can be considered to be composed of a stream of photons with each photon possessing an energy hc/λ, where h is Planck's constant and c is the speed of light. A basic concept of radiometry is that of the *spectral radiant power* $P(\lambda)$. Let light pass through a filter transmitting a spectral bandwidth $\Delta\lambda$ centered on λ and fall on a radiation detector. If the detector records N photons per second, the spectral radiant power is defined by

$$P(\lambda) = \frac{hc}{\lambda}\frac{N}{\Delta\lambda}. \tag{1}$$

The SI unit for $P(\lambda)$ is Watts/nm. In remote sensing it is important to record the direction in which the light is propagating as well as the associated power. This is accomplished with a quantity called the radiance. Consider a detector of spectral radiant power having an physical area A. Place a spectral filter, which passes a range of wavelengths $\Delta\lambda$ centered on λ, over the detector and equip the detector with an optical system which restricts its field of view to a small solid angle $\Delta\Omega$ (SI unit: Ster). Such an arrangement is called a radiometer. If the detector records a power $P(\lambda, \hat{\xi})$ when the radiometer aimed in a direction to receive photons traveling toward $\hat{\xi}$, it records, at its position, a *radiance* $L(\lambda, \hat{\xi})$ defined by

$$L(\lambda, \hat{\xi}) = \frac{P(\lambda, \hat{\xi})}{A\,\Delta\Omega\,\Delta\lambda}. \tag{2}$$

The SI unit for radiance is Watts/m^{2}nm Ster. In practice, $\Delta\Omega$ and $\Delta\lambda$ need to be sufficiently small so that a further reduction in their size does not change the radiance. All satellite and airborne ocean color remote sensing instruments measure spectral radiance.

Fundamental Quantities

The fundamental optical properties of a medium are defined and measured by probing samples of the medium with a well defined beam of light. Consider a small volume Δv of length Δl illuminated by a parallel beam of light traveling in a direction specified by the unit vector $\hat{\xi}$. Let $P_0(\lambda)$ be the radiant power entering the volume. As the photons pass through the volume some are removed from the beam by *absorption* within Δv. Others are removed from the parallel beam by a change in their direction (*scattering*) within Δv, and they will exit Δv traveling in directions

other than $\hat{\xi}$, e.g., $\hat{\xi}'$. If $\Delta P(\lambda)$ is the spectral radiant power removed from the parallel beam by virtue of scattering *and* absorption, then the *attenuation or extinction coefficient* $c(\lambda)$ is defined by

$$c(\lambda) = \frac{1}{\Delta l}\left[\Delta P(\lambda)/P_0(\lambda)\right]. \tag{3}$$

This is the fraction of the power removed from the beam per unit length. The SI unit for $c(\lambda)$ is m^{-1}. If $\Delta^2 P(\lambda, \hat{\xi}')$ is the spectral radiant power scattered into a small solid angle $\Delta\Omega(\hat{\xi}')$ containing the direction $\hat{\xi}'$, the *volume scattering function* $\beta(\lambda, \hat{\xi} \rightarrow \hat{\xi}')$ is defined according to

$$\beta(\lambda, \hat{\xi} \rightarrow \hat{\xi}') = \frac{1}{\Delta l\, \Delta\Omega(\hat{\xi}')}\left[\Delta^2 P(\lambda, \hat{\xi}')/P_0(\lambda)\right]. \tag{4}$$

The volume scattering function is the fractional power scattered from $\hat{\xi}$ into the direction $\hat{\xi}'$ per unit length per unit solid angle around $\hat{\xi}'$. [The "2" on $\Delta^2 P(\lambda, \hat{\xi}')$ indicates that it is of second order in smallness, i.e., small because Δl is small and also small because $\Delta\Omega(\hat{\xi}')$ is small.] β is the differential scattering cross section per unit volume. The SI unit for β is $m^{-1}Ster^{-1}$. In Eqs. (3) and (4) Δl and $\Delta\Omega(\hat{\xi})$ must be sufficiently small that photons have a negligible probability of scattering more than once in Δv. For particles in random orientation, β depends on direction only through the angle α between $\hat{\xi}$ and $\hat{\xi}'$ given by $\alpha = \cos^{-1}(\hat{\xi} \bullet \hat{\xi}')$. If we sum the contributions from each $\Delta\Omega(\hat{\xi}')$ over the entire sphere surrounding Δv, i.e., sum the light scattered into all directions, the result is called the *scattering coefficient* $b(\lambda)$:

$$b(\lambda) = \int_{4\pi} \beta(\lambda, \hat{\xi} \rightarrow \hat{\xi}')d\Omega(\hat{\xi}'). \tag{5}$$

The 4π on the integral in Eq. (5) means that it is to be taken over 4π Ster. The scattering processes we deal with here are *elastic*, i.e., there is no wavelength (energy) change upon scattering. Finally, since light that is removed from the beam, but not scattered, must have been absorbed, we can define *absorption coefficient* $a(\lambda)$ through

$$a(\lambda) = c(\lambda) - b(\lambda). \tag{6}$$

The quantities $a(\lambda)$, $b(\lambda)$, $c(\lambda)$, and $\beta(\lambda, \hat{\xi} \rightarrow \hat{\xi}')$ are referred to as the inherent optical properties (IOP's) of the atmosphere[6,7]. From the definitions of the IOP's (which require the absence of multiple interactions within Δv) they must be additive over the constituents of the medium. It is useful to introduce two auxiliary IOP's: the single scattering albedo

$$\omega_0(\lambda) = \frac{b(\lambda)}{c(\lambda)},$$

which is the probability that when a photon interacts with the atmosphere it will be scattered; and the scattering phase function

$$P(\lambda, \hat{\xi}' \rightarrow \hat{\xi}) = \frac{\beta(\lambda, \hat{\xi}' \rightarrow \hat{\xi})}{b(\lambda)},$$

i.e., the VSF normalized to the total scattering coefficient.

Absorption and scattering in the atmosphere is usually very small and measurements of the optical properties are often carried out utilizing very long paths, i.e., kilometers. A measurement

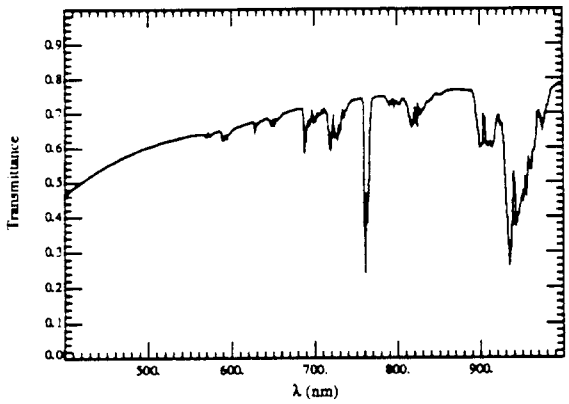

Figure 1. Vertical path transmittance of the atmosphere including the contributions of air, water vapor, and Ozone.

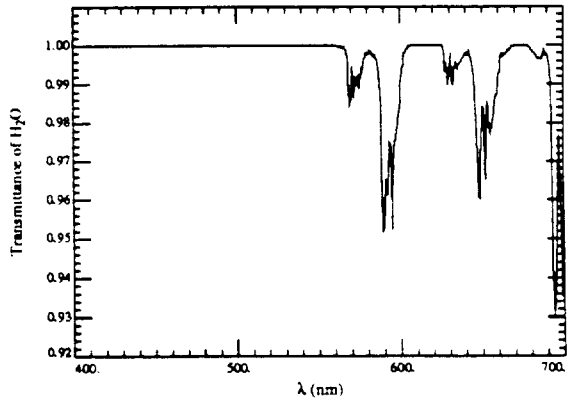

Figure 2. Contribution to the vertical path transmittance of the atmosphere by water vapor absorption alone.

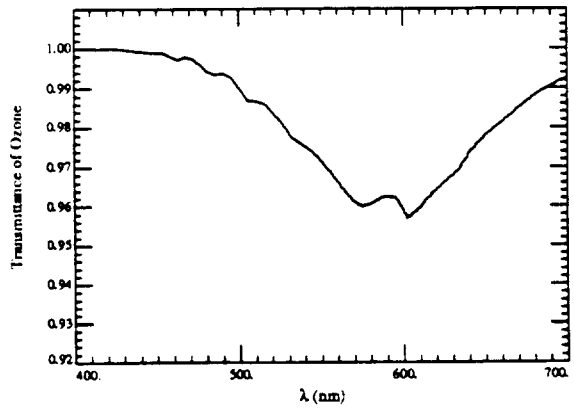

Figure 3. Contribution to the vertical path transmittance of the atmosphere by Ozone absorption alone.

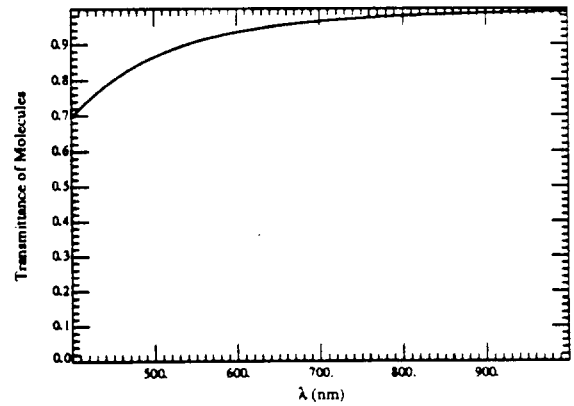

Figure 4. Contribution to the vertical path transmittance of the atmosphere by molecular scattering alone.

of particular importance is the transmittance. Let a radiometer view an extended source, e.g., the

sun. Then the *transmittance* T of the path between the source and the observer is defined to be the measured radiance (L_m) divided by the radiance of the source (L_s):

$$T = \frac{L_m}{L_s}.$$

We shall see later that if there is no absorption or scattering over the path the transmittance is unity. If there are N scattering and absorbing species in the path, then $T = \prod_{i=1}^{N} T_i$, where T_i is the transmittance of the i^{th} constituent alone. Much information concerning the optical properties of the atmosphere is obtained by measuring its transmittance using the sun as a source.

Optical Properties of the Atmosphere

The atmospheric constituents that produce significant absorption in the visible portion of the spectrum are O_2, O_3, and H_2O. An example of the transmission of the atmosphere from 400 to 1000 nm looking toward the zenith, derived using LOWTRAN 7* for a particular model of the atmosphere (the 1976 U.S. Standard Atmosphere[9]), is provided in Figure 1. Figure 1 includes the effects of all of the gases above as well as scattering by molecules and the aerosols (small particles suspended in the air). The absorption features near 686 nm and 759 nm are due to O_2. The rest of the distinct features are due to H_2O, with the exception of a weak absorption by O_3 extending through most of the visible spectrum. The individual transmittances of H_2O and O_3 in the visible, derived from LOWTRAN 7, is shown in Figures 2 and 3, respectively. Clearly, it is desirable to place the spectral bands on ocean color remote sensing instruments away from the absorption bands of atmospheric gases, particularly gases with highly variable concentrations, e.g., H_2O and O_3. However, this is not always possible (Figure 3).

The transmittance in Figure 1 is also affected by scattering by the atmospheric constituents. The scattering of light by the molecules themselves is referred to as *Rayleigh* scattering. The volume scattering function for Rayleigh scattering is

$$\beta_r(\alpha) = b_r \frac{3}{8\pi}\left[\frac{1-\delta}{2+\delta}\right]\left[1 + \frac{1-\delta}{1+\delta}\cos^2\alpha\right],$$

* LOWTRAN 7 is a computer program developed at the U.S. Air Force Geophysics Laboratory. It combines the results of laboratory measurements on gases of interest in the atmosphere with climatological mean vertical distributions of the gases and other constituents to allow one to compute the transmittance of the atmosphere for any path.[8]

where b_r is the total scattering coefficient (proportional to the density of the air) and δ is the depolarization ratio, the ratio of the radiance scattered at $\alpha = 90°$ with polarization parallel to that with polarization perpendicular to the scattering plane, when the incident beam is unpolarized. Its value is taken by Hansen and Travis[10] to be $\delta = 0.031$. From the form of β_r we see that Rayleigh scattering is symmetric with respect to a scattering angle of 90°, i.e., $\beta(\alpha) = \beta(\pi - \alpha)$. The *optical thickness* for Rayleigh scattering in the atmosphere is defined by

$$\tau_r \equiv \int_0^\infty b_r(h)dh \tag{7}$$

where h is altitude. Hansen and Travis[10] give

$$\tau_{r_0} = 0.008569\lambda^{-4}\left(1 + 0.0113\lambda^{-2} + 0.00013\lambda^{-4}\right), \tag{8}$$

where τ_{r_0} is the optical thickness at the standard atmospheric pressure P_0 of 1013.25 mb and λ is the wavelength in μm. Note that τ_{r_0} varies nearly as λ^{-4} with wavelength. Since b_r is $\propto$ the air density, τ_r will be $\propto$ the surface pressure, i.e., at any surface pressure P,

$$\tau_r = \frac{P}{P_0}\tau_{r_0}. \tag{9}$$

Figure 4 shows the effect of Rayleigh scattering on the transmittance in the visible part of the spectrum.

The transmittance is also influenced by scattering by aerosols — solid and/or liquid particles suspended in the air. In fact, in the "windows" between the absorption features in Figure 1, the attenuation is due to a combination of molecular scattering and aerosol attenuation. Since molecular scattering only weakly influences the transmittance in the red (Figure 4), most of the attenuation in the windows there is due to aerosols. For aerosol particles, the value of ω_0 is typically near unity so their principal effect in the atmosphere is to scatter light. We will need to understand the scattering properties of the aerosol and their variability.

Aerosols are typically modeled as a collection of homogeneous spheres with a range of sizes. If we let D represent the diameter of the particles, and $dn(D)$ the number of particles per unit volume with diameters between D and $D + dD$, then the *size distribution* is defined to be $dn(D)/dD$. If N is the total number of particles per unit volume, i.e.,

$$N = \int_0^\infty \frac{dn(D)}{dD}\, dD,$$

then the *normalized* size distribution or *size frequency distribution* is defined to be $dn(D)/NdD$. The electromagnetic parameter that governs the optical properties of the particles is the complex index of refraction, $m = n_r - in_i$, where n_r is the real part of the index and governs refraction, and n_i is the imaginary part of the index and is proportional to the absorption coefficient a_m of the material of which the particle is composed ($n_i = a_m\lambda/4\pi$). Given $dn(D)/NdD$, the fact that the particles are assumed to be *homogeneous* and *spherical*, and their refractive index m, it is possible to compute their scattering and absorbing properties from Mie theory.[11–13] To demonstrate some of the properties of the aerosol scattering and absorption, I have computed the scattering phase functions for particles distributed according to

$$\begin{aligned} \frac{dn(D)}{dD} &= K, & D_0 < D < D_1, \\ &= K\left(\frac{D_1}{D}\right)^{\nu+1}, & D_1 < D < D_2, \\ &= 0, & D > D_2. \end{aligned}$$

The parameters D_0, D_1, D_2, ν, and m are provided in Table 1. (Note that $N \propto K$, so K is not specified.) These models define what I refer to as an *aerosol type*, i.e., $dn(D)/NdD$ and m. The

Table 1. Parameters of the Aerosol Models

Model	D_0 (μm)	D_1 (μm)	D_2 (μm)	ν	m
Haze C	0.06	0.20	20.0	2.5-4	1.50
Haze C	0.06	0.20	20.0	2.5-4	1.33
HMF7	0.20	0.40	17.5	2.95	$1.45 - 0.020i$
HMF9	0.20	0.60	17.5	2.95	$1.37 - 0.004i$

models with $m = 1.50$ define a typical continental aerosol,[14] while those with $m = 1.333$ refer to a continental aerosol size distribution composed of water particles. To model a marine aerosol (very small and very large particles missing) I have chosen size distributions and refractive indices similar to Quenzel and Kastner.[15] HMF7 models an aerosol for a relative humidity of 70%, while HMF9 models an aerosol for a relative humidity of 90%. Note the increased water content (m closer to that of water) and the particle swelling which takes place as the relative humidity increases from 70 to 90%.

Samples of the computed scattering phase functions at 670 nm are shown in Figures 5 and 6 for the continental aerosol models. We note that these phase functions are very strongly peaked in

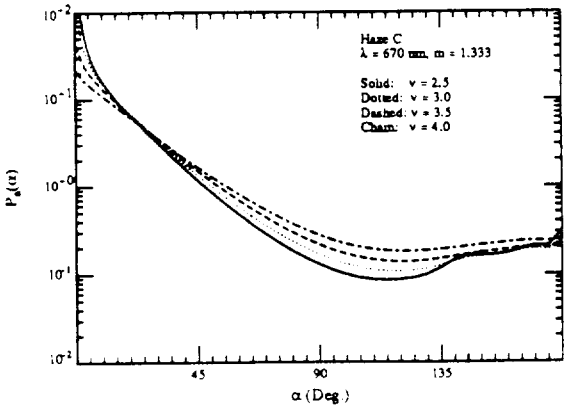

Figure 5. Aerosol phase functions for the Haze C model with $m = 1.333$.

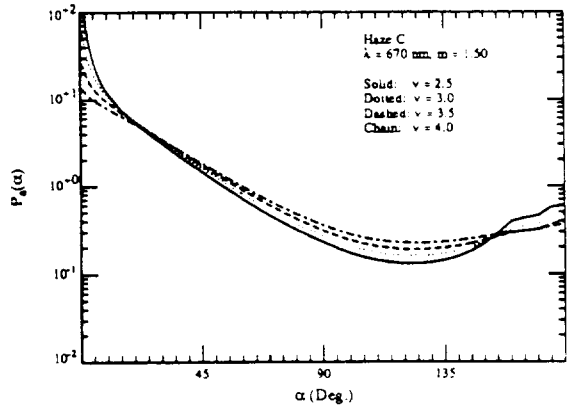

Figure 6. Aerosol phase functions for the Haze C model with $m = 1.50$.

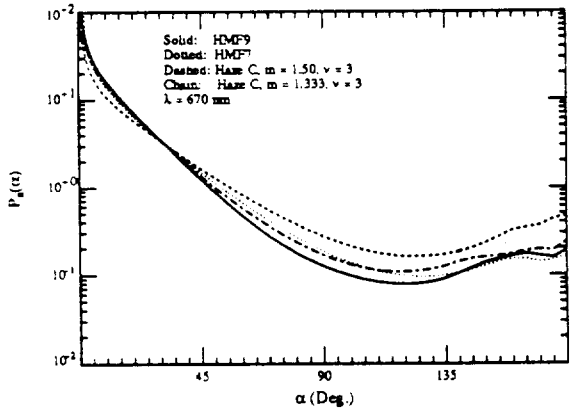

Figure 7. Aerosol phase functions for the marine aerosol models.

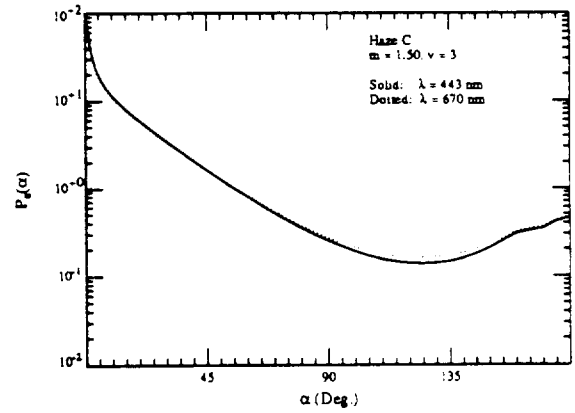

Figure 8. Aerosol phase functions for the Haze C model with $m = 1.50$ and $\nu = 3$.

the forward direction ($\alpha = 0°$). As the particle size distributions become more concentrated toward smaller particle sizes (larger ν), the phase function shows less pronounced forward scattering and more enhanced scattering at angles greater than about 30°. However, for $m = 1.50$ the back scattering, i.e., $\alpha \gtrsim 150°$ is more pronounced for the distributions favoring the larger particle sizes. Figure 7 compares all of the models, with $\nu \approx 3$, at 670 nm, providing examples of how the phase function changes with m for models with nearly the same size distribution. (Note, however, that unlike the marine aerosol models, the Haze C distributions have particles in the size range $0.06 \leq D \leq 0.2$ μm.) It suggests that even when the size distribution is known, a realistic range of

refractive indices can result in the variation of $P_a(\alpha)$ of over a factor of two for $\alpha \gtrsim 45°$. Figures 8 and 9 show examples of the variation of the aerosol phase function with wavelength. Clearly, the aerosol phase function depends only *weakly* on wavelength throughout the visible. One might

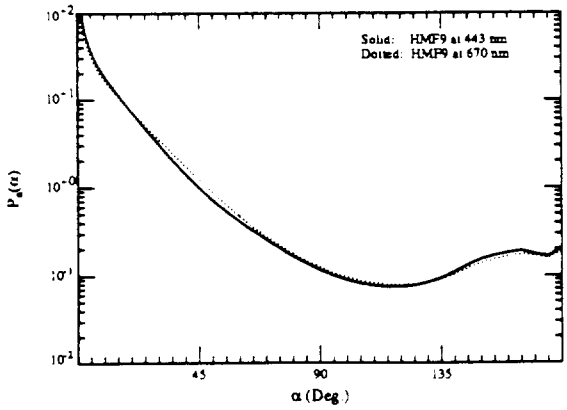

Figure 9. Aerosol phase functions for the HMF9 marine model.

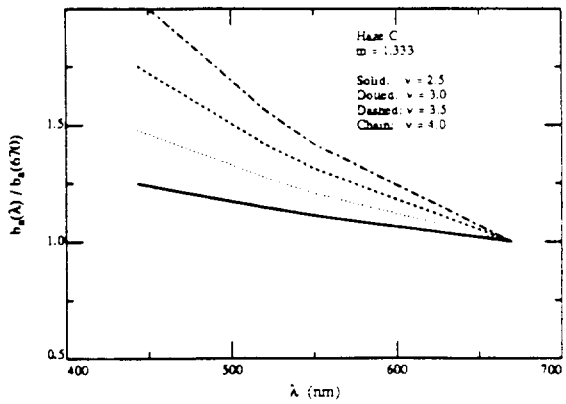

Figure 10. Spectral variation of b_a for the Haze C models with $m = 1.333$.

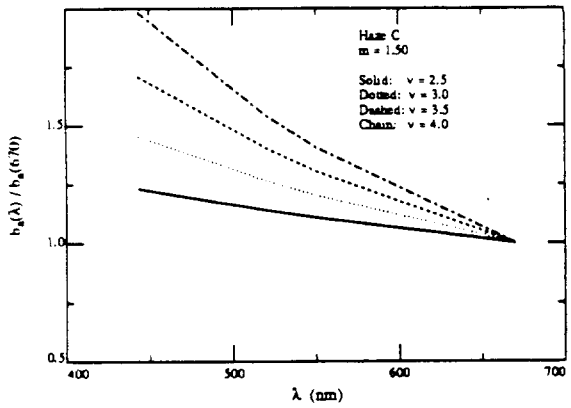

Figure 11. Spectral variation of b_a for the Haze C models with $m = 1.50$.

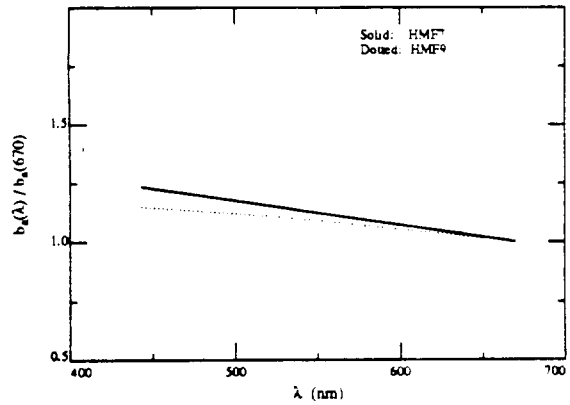

Figure 12. Spectral variation of the aerosol scattering coefficient for the marine aerosol models.

expect that the phase function should increase with wavelength for angles greater than about 30°, since the particle's diameter becomes a smaller fraction of the wavelength. The Haze C model follows this (Figure 8); however, in the case of the marine aerosol this tendency is reversed for angles greater than about 150° (Figure 9).

Figures 10, 11, and 12 provide the computations of the variation of the scattering coefficient b_a with λ, i.e., the quantity $b_a(\lambda)/b_a(670)$ for $\lambda = 443$, 520, 550, and 670 nm. If the aerosol *type* is

independent of altitude, and the aerosol is *nonabsorbing*, this is

$$\frac{b_a(\lambda)}{b_a(670)} = \frac{\tau_a(\lambda)}{\tau_a(670)},$$

where $\tau_a(\lambda)$ is the optical thickness of the aerosol component. These figures suggest that

$$\frac{\tau_a(\lambda)}{\tau_a(670)} \approx \left(\frac{670}{\lambda}\right)^n, \tag{10}$$

where for both the Haze C models $n \approx \nu - 2$. Furthermore, for this range of refractive indices, the spectral variation of b_a is more strongly influenced by the size distribution than by the actual value of m (compare Figures 10 and 11).

It was mentioned earlier that ω_0 for the aerosols is near unity. In fact, if $n_i = 0$, i.e., the refractive index is real, there is no absorption and $\omega_0 = 1$, exactly, otherwise, $\omega_0 < 1$. Thus, the Haze C aerosol models here have $\omega_0 = 1$. For the marine aerosol models, the Mie computations provide

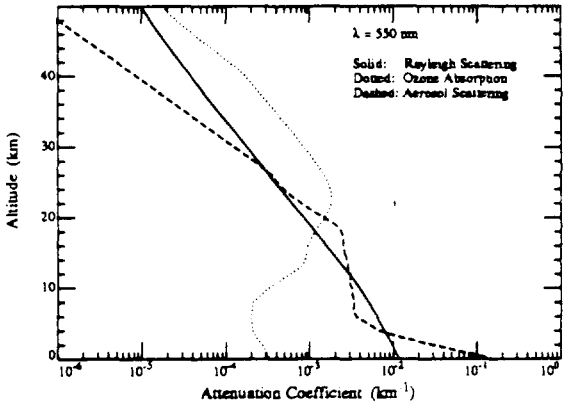

Figure 13. Vertical distribution of the attenuation coefficient of air, aerosols, and O_3.

$0.832 \leq \omega_0(\lambda) \leq 0.843$ for HMF7 and $0.939 \leq \omega_0(\lambda) \leq 0.950$ for HMF9, with $443 \leq \lambda \leq 670$. Note the model with the larger $|n_i|$ yields smaller ω_0. These computations suggest that as long as n_i is constant, $\omega_0(\lambda)$ will vary very little with λ over the visible spectrum.

The above models are introduced to provide examples of the scattering properties of the aerosols and their variation. More sophisticated models of the aerosol now exist (see for example the aerosol models in LOWTRAN 7); however, the simple models I have discussed provide sufficient background to understand the influence of aerosols on ocean color remote sensing.

Finally, we consider the vertical distribution of the optically important constituents. To compare one component with another it is more instructive to use profiles of attenuation rather than concentration. This is effected in Figure 13, which provides the attenuation coefficient of air, aerosols, and O_3. These species are distributed with altitude according to mean profiles determined by Elterman.[16] Water vapor is not considered since ocean color sensors avoid the water vapor bands. It is seen that the aerosols provide the dominant attenuation near the surface, Rayleigh scattering above the immediate surface layer, and O_3 above about 20 km. It is important to note that the aerosol profile can differ significantly from that in the figure. For example, a major volcanic eruption, such as El Chichón in 1982, can eject enough aerosol into the stratosphere that the aerosol, rather than O_3, determines the optical properties there. It is rare, however, that the aerosol concentration is not largest near the surface.

Radiative Transfer

Consider a cartesian coordinate system with its origin at the "top" of the atmosphere. The x and y axes parallel to a plane tangent to the earth's surface below the origin and the z axis is directed toward the earth. A photon's direction is specified by the polar angle (θ) and the azimuth angle (ϕ) of a spherical coordinate system built on the cartesian system, i.e., if a photon is traveling in the direction specified by the unit vector $\hat{\xi}$, the components of $\hat{\xi}$ are $(x, y, z) = (\sin\theta\cos\phi, \sin\theta\sin\phi, \cos\theta)$. Thus, photons traveling toward the earth have $0 \leq \theta < 90°$, while photons traveling toward space have $90 < \theta \leq 180°$. The atmosphere is assumed to be plane parallel and horizontally homogeneous, so L is taken to be a function of altitude, direction, and wavelength, i.e., $L = L(z, \theta, \phi, \lambda)$.

The Radiative Transfer Equation

The propagation of radiance is governed by the radiative Transfer equation (RTE). In an atmosphere in which the IOP's depend only on altitude, the RTE is

$$\cos\theta \frac{dL(z,\lambda,\theta,\phi)}{dz} = -c(z,\lambda)L(z,\lambda,\theta,\phi) + \int_{4\pi} \beta(z,\lambda,\theta',\phi' \rightarrow \theta,\phi)L(z,\lambda,\theta',\phi')\,d\Omega', \qquad (11)$$

where $d\Omega' = \sin\theta'\,d\theta'\,d\phi'$, and the 4π on the integral means that the integration is to be carried out over all θ' and ϕ'. The first term on the right-hand-side represents the loss of radiance in the direction (θ, ϕ) by scattering and absorption. The second term is the gain in radiance due to scattering of radiance from all other directions (θ', ϕ') into the direction (θ, ϕ). In this formulation

the polarization of the light is ignored. In what follows, we shall omit the explicit dependence of the various quantities on λ except where necessary to avoid confusion. In terms of these auxiliary IOP's, ω_0 and P, the RTE becomes

$$\cos\theta \frac{dL(z,\theta,\phi)}{c(z)dz} = -L(z,\theta,\phi) + \omega_0(z) \int_{4\pi} P(z,\theta',\phi' \rightarrow \theta,\phi) L(z,\theta',\phi')\, d\Omega'. \tag{12}$$

Case[17] has shown that, given the radiance incident on the upper and lower boundaries of the atmosphere, the solutions to the RTE are unique if $\omega_0 < 1$, i.e., there is *some* absorption. Note that in Eq. (12), $c(z)$ occurs only in the combination $c(z)\,dz$, so a dimensionless depth τ — the *optical depth* — such that $d\tau = c(z)\,dz$, is introduced. In a homogeneous atmosphere, $\tau = cz$, and the RTE becomes

$$\cos\theta \frac{dL(\tau,\theta,\phi)}{d\tau} = -L(\tau,\theta,\phi) + \omega_0 \int_{4\pi} P(\theta',\phi' \rightarrow \theta,\phi) L(\tau,\theta',\phi')\, d\Omega', \tag{13}$$

Analytical solutions to the RTE are possible only in the simplest case, e.g., $\omega_0 = 0$, so one must be satisfied with numerical solutions.

The Successive Order of Scattering Solution

The successive order of scattering technique is the most straightforward technique for solving the RTE. The basic idea is to successively compute the radiance that is scattered once, twice, etc., and then to sum these contributions to obtain the total radiance.[10,18] The development is simplified if we consider a homogeneous atmosphere with $\omega_0 < 1$. We then assume that the radiance can be expanded in a power series in ω_0,[19] i.e.,

$$L(\tau,\theta,\phi) = L^{(0)}(\tau,\theta,\phi) + \omega_0 L^{(1)}(\tau,\theta,\phi) + \omega_0^2 L^{(2)}(\tau,\theta,\phi) + \cdots,$$

put this into the RTE, and group like powers of ω_0. The RTE is then satisfied if the individual $L^{(n)}$'s satisfy

$$\begin{aligned}
\cos\theta \frac{dL^{(0)}}{d\tau} &= -L^{(0)}, \\
\cos\theta \frac{dL^{(1)}}{d\tau} &= -L^{(1)} + \int P L^{(0)\prime}\, d\Omega', \\
\cos\theta \frac{dL^{(2)}}{d\tau} &= -L^{(2)} + \int P L^{(1)\prime}\, d\Omega', \\
&\vdots \\
\cos\theta \frac{dL^{(n)}}{d\tau} &= -L^{(n)} + \int P L^{(n-1)\prime}\, d\Omega', \\
&\vdots
\end{aligned} \tag{14}$$

These represent a simplification in that the single integral-differential equation has been transformed into a set of ordinary differential equations (the integrals can now be evaluated in principle since each integrand is furnished by solving the preceding equation). If the atmosphere is illuminated from above by a radiance $L_{\text{inc}}(0,\theta,\phi)$, we will choose the simplest way of satisfying the boundary condition at $z = 0$:

$$L^{(0)}(0,\theta,\phi) = L_{\text{inc}}(0,\theta,\phi)$$

$$L^{(n)}(0,\theta,\phi) = 0 \quad \text{for } n > 0.$$

In the case of interest, the atmosphere is bounded below by a Fresnel-reflecting sea surface. If the surface is *flat*, the lower boundary condition (at $z = z_1$) is

$$L^{(n)}(z_1,\theta_r,\phi_r) = \rho(\theta_i)L^{(n)}(z_1,\theta_i,\phi_i) \qquad \text{for all } n, \tag{15}$$

where (θ_i,ϕ_i) is the direction of the incident photon, (θ_r,ϕ_r) is the direction of the reflected photon ($\theta_r = \pi - \theta_i$, $\phi_r = \phi_i$), and $\rho(\gamma)$ is the Fresnel reflectance of the flat ocean surface for an incident angle of γ with respect to the normal. It is given by

$$\rho(\gamma) = \frac{1}{2}\left[\frac{\tan^2(\gamma-\gamma')}{\tan^2(\gamma+\gamma')} + \frac{\sin^2(\gamma-\gamma')}{\sin^2(\gamma+\gamma')}\right],$$

where γ and γ' are related by Snell's law: $m_w \sin\gamma' = \sin\gamma$, with m_w representing the index of refraction of water.

The Single Scattering Approximation

In the *single scattering* approximation the series is terminated at $n = 1$, i.e., $L = L^{(0)} + \omega_0 L^{(1)}$. We will now develop this solution for a homogeneous atmosphere with no upward radiance incident on the lower boundary, which we take to be located at $z = z_1$ or $\tau = \tau_1$. The radiance incident on the top of the atmosphere is that due to the solar beam, i.e.,

$$L_{\text{inc}}(0,\theta,\phi) = F_0\delta(\cos\theta - \cos\theta_0)\delta(\phi - \phi_0), \tag{16}$$

where θ_0 and ϕ_0 are the solar zenith and azimuth angles, respectively, and δ is the Dirac delta function. F_0 is the solar irradiance (the power per unit area per unit $\Delta\lambda$) on a plane normal to the sun's rays at the top of the atmosphere. It depends on the position of the earth in its orbit and is given by

$$F_0(\lambda) = \langle F_0(\lambda)\rangle \left(1 + 0.016\cos\left[\frac{2\pi(D-3)}{365}\right]\right)^2,$$

where D is the day of the year ($D = 1$ on 1 Jan. and $D = 365$ on 31 Dec.). $\langle F_0 \rangle$ as a function of wavelength, measured by Neckel and Labs,[20] is presented in Figure 14. The equation for $L^{(0)}$ can be solved immediately yielding

$$L^{(0)}(\tau, \theta, \phi) = F_0 \delta(\cos\theta - \cos\theta_0)\delta(\phi - \phi_0)\exp(-\tau/\cos\theta_0). \tag{17}$$

Note that the transmittance defined earlier is given by $T(\theta_0, \phi_0) = \exp(-\tau/\cos\theta_0)$, and measure-

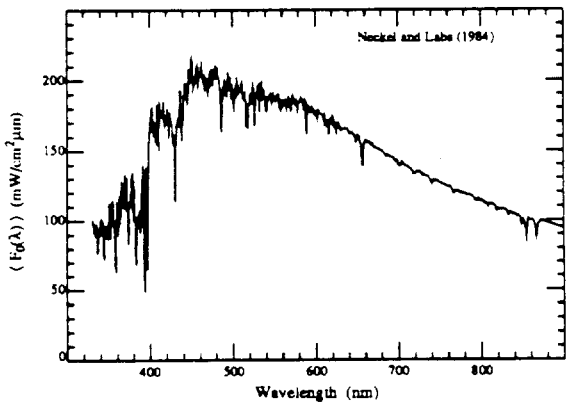

Figure 14. Mean extraterrestrial solar irradiance.

ment of T yields τ, the optical thickness of the atmosphere. The equation for $L^{(1)}$ then becomes

$$\begin{aligned}\cos\theta \frac{dL^{(1)}}{d\tau} &= -L^{(1)} + \int P L^{(0)\prime}\, d\Omega' \\ &= -L^{(1)} + P(\theta_0, \phi_0 \rightarrow \theta, \phi) F_0 \exp(-\tau/\cos\theta_0).\end{aligned}$$

The solution to this equation for the radiance in the atmosphere is

$$\begin{aligned}L_u^{(1)}(\tau, \theta, \phi) = &\frac{F_0 \cos\theta_0 P(\alpha)}{\cos\theta_0 - \cos\theta} \exp(-\tau/\cos\theta) \\ &\times \Big(\exp[+\tau(1/\cos\theta - 1/\cos\theta_0)] - \exp[+\tau_1(1/\cos\theta - 1/\cos\theta_0)]\Big)\end{aligned} \tag{18}$$

and

$$L_d^{(1)}(\tau, \theta, \phi) = \frac{F_0 \cos\theta_0 P(\alpha)}{\cos\theta_0 - \cos\theta}\Big(\exp[-\tau/\cos\theta_0] - \exp[-\tau/\cos\theta]\Big), \tag{19}$$

where

$$\cos\alpha = \cos\theta\cos\theta_0 + \sin\theta\sin\theta_0\cos\phi,$$

and ϕ_0 is taken to be zero, i.e., the sun's rays are parallel to the x-z plane. The subscripts u and d in Eqs. (18) and (19) mean "up" ($\theta > 90°$) and "down" ($\theta < 90°$), respectively. To this order,

$L = L^{(0)} + \omega_0 L^{(1)}$, so if $\theta \neq \theta_0$, $L_u(\tau, \theta, \phi)$ and $L_d(\tau, \theta, \phi)$ are given by Eqs. (18) and (19) with P replaced by $\omega_0 P$, respectively. If the atmosphere is "optically thin," i.e., $\tau_1 \ll 1$, the exponentials can be expanded in a power series in τ_1 to obtain,

$$\begin{aligned} L_u(0, \theta, \phi) &= -\frac{F_0 \omega_0 P(\alpha) \tau_1}{\cos\theta}, \qquad \theta > 90^\circ \\ L_d(\tau_1, \theta, \phi) &= +\frac{F_0 \omega_0 P(\alpha) \tau_1}{\cos\theta}, \qquad \theta < 90^\circ. \end{aligned} \tag{20}$$

Thus, the radiance exiting a thin layer of atmosphere is directly proportional to $\omega_0 P(\alpha)\tau_1$.

Now we consider the case of a thin atmosphere bounded below by a specularly reflecting, flat ocean surface. (We ignore for the present the contribution to the radiances from photons which are backscattered *out* of the ocean.) We wish to compute the radiance leaving the atmosphere $L_u(0, \theta, \phi)$. Equation (20) provides the contribution to $L_u(0, \theta, \phi)$ from single scattering of the direct solar beam in the medium; however, there are two other single scattering contributions to $L_u(0, \theta, \phi)$. The solar beam can first scatter in the atmosphere generating $L_d(\tau_1, \theta, \phi)$ at the lower boundary which is then Fresnel-reflected by the sea surface back into the atmosphere and propagates to the top. Alternatively, the solar beam can propagate to the surface without scattering, Fresnel-reflect from the sea surface back into the atmosphere, scatter in the atmosphere toward the direction (θ, ϕ) and propagate to the top. In the thin layer approximation (first order in τ_1) these two processes yield a contribution to $L_u(0, \theta, \phi)$ of

$$-\frac{F_0 \omega_0 P(\alpha_-)\tau_1}{\cos\theta}\left[\rho(\theta) + \rho(\theta_0)\right],$$

where

$$\cos\alpha_- = -\cos\theta\cos\theta_0 + \sin\theta\sin\theta_0\cos\phi.$$

Thus, for a thin homogeneous atmosphere of optical thickness τ_1 with a Fresnel reflecting lower boundary, the radiance leaving the top of the atmosphere is, to first order in τ_1,

$$L_u(0, \theta, \phi) = -\frac{F_0 \omega_0 \tau_1}{\cos\theta}\Big(P(\alpha_+) + [\rho(\theta) + \rho(\theta_0)]P(\alpha_-)\Big), \tag{21}$$

where

$$\cos\alpha_\pm = \pm\cos\theta\cos\theta_0 + \sin\theta\sin\theta_0\cos\phi.$$

Note that $\omega_0 P \tau_1$ is just βz_1, so if there are several scattering constituents in the atmosphere, the

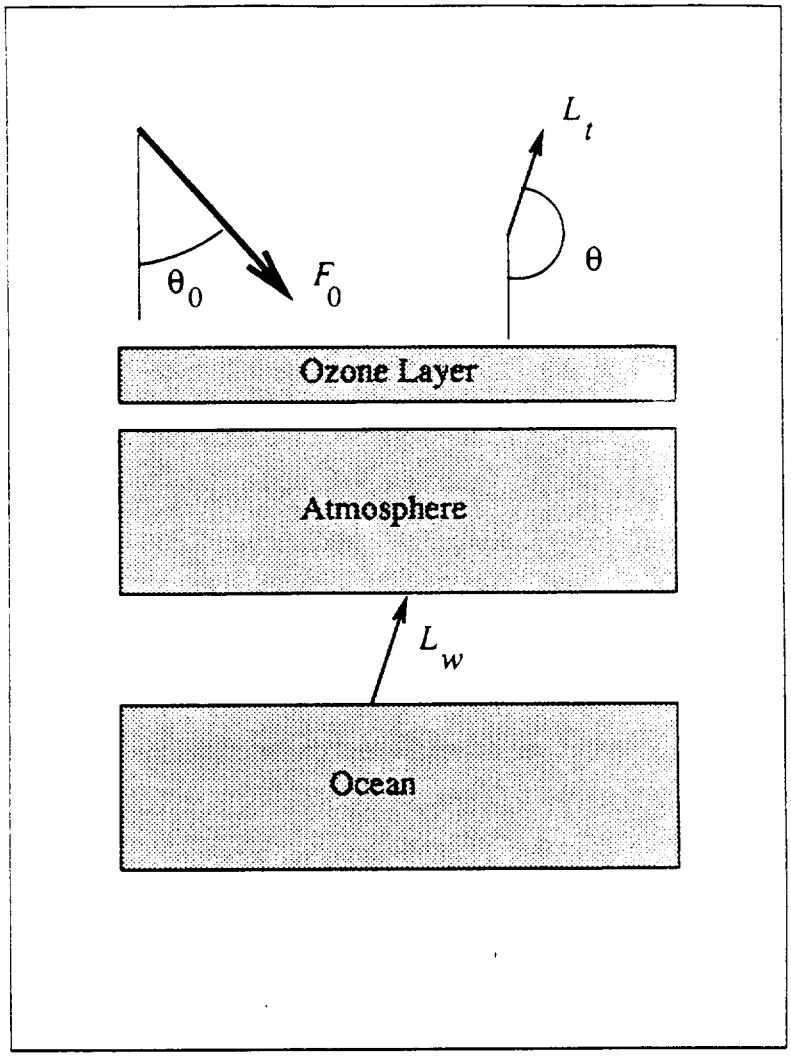

Figure 15. Schematic of the sensing geometry.

contributions from each are linearly additive in the single scattering approximation (note that each component will have a different τ_1).

First Order Radiance Model for Atmospheric Correction

We can use the approximation of an optically thin atmosphere to model the ocean color remote sensing situation depicted schematically in Figure 15. To effect this we must calculate the radiance reflected from the atmosphere-ocean system. Consider first just the atmosphere and the flat air-sea

interface. In this case, we can use Eq. (21) to estimate the upward radiance at the top of the atmosphere resulting from scattering by molecules and aerosols. This is

$$L_r + L_a$$

with

$$L_x(0,\theta,\phi) = -\frac{F_0\omega_x\tau_x}{\cos\theta}\Big(P_x(\alpha_+) + [\rho(\theta)+\rho(\theta_0)]P_x(\alpha_-)\Big), \tag{22}$$

where x refers to the particular component, i.e., $x = r$ or a for the "Rayleigh" and aerosol components, respectively. However, this radiance is not correct because the influence of O_3 has been ignored. In Figure 13 we see that the major contribution from O_3 comes at altitudes above 20 to 25 km, where the Rayleigh and aerosol scattering coefficients are small. Thus, a simple way to include O_3 in this first order model is to confine it in a layer above the thin atmosphere. The scattered radiance will then have to make two trips through the O_3 layer to reach the receiver as shown in Figure 15. This will attenuate the radiance by a factor

$$\exp\big[-\tau_{Ox}(1/\cos\theta_0 - 1/\cos\theta)\big]; \qquad \theta > 90°,$$

where τ_{Ox} is the optical thickness of O_3 in the atmosphere. Thus, the radiances given above can be modified to include O_3 by letting

$$F_0 \rightarrow F_0' = F_0\exp\big[-\tau_{Ox}(1/\cos\theta_0 - 1/\cos\theta)\big]; \qquad \theta > 90°. \tag{23}$$

Another component of the radiance at the top of the atmosphere is due to the reflection of the direct solar beam from the sea surface, and its subsequent transmission to the top of the atmosphere. It is given by

$$L_g(0,\theta,\phi) = F_0\rho(\theta_0)\delta(\theta+\theta_0-\pi)\delta(\phi)\exp\big[-\tau(1/\cos\theta_0 - 1/\cos\theta)\big],$$

where $\tau = \tau_r + \tau_a + \tau_{Ox}$ is the total optical thickness of the atmosphere. The subscript "g" is used for this component since, when the sea surface is ruffled by the wind (and no longer flat), this term will produce what is commonly called sun glint. Finally, there is a component of the radiance due to light that has been backscattered *out* of the water. At the sea surface this component is called the *water-leaving radiance*, L_w. In propagation to the top of the atmosphere, it is attenuated by a factor t yielding tL_w at the sensor. The attenuation factor t depends on the angular distribution of L_w. If L_w were large in a single direction (like $L_{\rm inc}$ at the top of the atmosphere) then t would be the "direct" transmittance (similar to $T(\theta_0,\phi_0)$). If L_w were totally diffuse, i.e., if L_w were

independent of θ and ϕ, then t would be the transmittance function for irradiance,[21-23] i.e., the *diffuse* transmittance. Irradiance is defined to be the spectral radiant power per unit area per $\Delta\lambda$ falling on a horizontal surface. Since L_w is much closer to being totally diffuse than beam-like, we use the diffuse transmittance for t. It is given by[24]

$$t = \exp\left[(\tau_r/2 + \tau_{Oz})/\cos\theta\right] t_a, \qquad \theta > 90°,$$

where

$$t_a \cong \exp\left[(1 - \omega_a F_a)\tau_a/\cos\theta\right], \tag{24}$$

and F_a is the probability that a photon scattered by the aerosol will be scattered through an angle less than 90°. The total radiance at the top of the atmosphere, L_t, is then

$$L_t = L_r + L_a + L_g + tL_w. \tag{25}$$

The basic problem of atmospheric correction is to extract L_w from L_t. To provide an appreciation for the importance (and difficulty) of atmospheric correction, we present in Figure 16 simulated spectra of the total radiance L_t at the top of the atmosphere and the desired water-leaving radiances

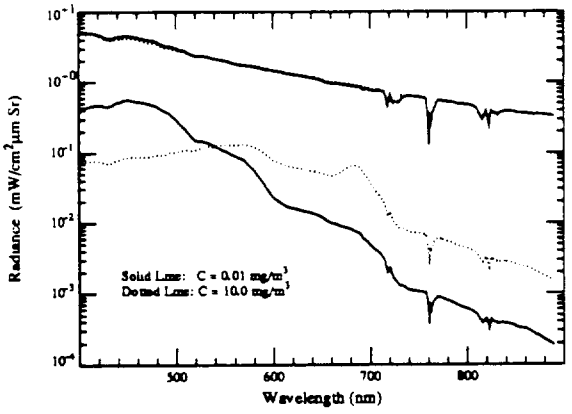

Figure 16. Simulated spectra of the upward radiance at the sea surface (lower curves) and the top of the atmosphere (upper curves) for low (solid) and high (dotted) pigment concentrations.

L_w for low and high pigment concentrations in Case 1 waters.[25*] We note that the variations in

* Case 1 waters[26,27] are defined to be waters for which the optical properties are controlled principally by the water itself and/or by phytoplankton and their immediate degradation products. The optical properties of the biogeneous component can be parameterized by the pigment concentration.[27,28] The pigment concentration is defined to be the sum of the concentrations (in mg/m^3) of chlorophyll *a* and phaeophytin *a*.

L_w are nearly masked by the atmospheric scattering in L_t. Also, we see that for low pigment concentrations L_w ranges from about 15% of L_t in the blue to 1% in the red, while for the high pigment concentration the range is from about 2% in the blue to as much as 5% in the red. In the near infrared (NIR) L_w is always less than 1% of L_t. Algorithms for extracting pigment concentration from ocean color measurements usually use the ratio of L_w's in the blue and green regions of the spectrum,[26,27,29,30] e.g., in the case of CZCS (spectral bands at 443, 520, 550, and 670 nm, referred to as λ_1, λ_2, λ_3, and λ_4, respectively) the pigment concentration is estimated from the ratios

$$r_{1,3} = \frac{L_w(\lambda_1)}{L_w(\lambda_3)} \qquad \text{and/or} \qquad r_{2,3} = \frac{L_w(\lambda_2)}{L_w(\lambda_3)}. \tag{26}$$

Since the red and NIR portions are least affected by L_w it is natural to use this spectral region to assess the effects of the atmosphere and sea surface.

To estimate L_w in Eq. (25) we need estimates of L_r, L_g and L_a. Knowing the optical thicknesses τ_r and τ_{Oz}, we can compute L_r using Eq. (22). We note that τ_r depends on wavelength as given in Eq. (8) and on the surface atmospheric pressure as in Eq. (9). Gordon, Brown, and Evans[31] show that the neglect of the surface pressure variations will result in at most an error of $\pm 1.5\%$ and usually much less, and at this point we will ignore the surface pressure variation. Also, although the O_3 concentration varies significantly in space and time, at this point we will simply use a climatological mean to determine τ_{Oz}.

L_g in Eq. (25) is large only near the specular image of the sun, i.e., for a flat sea surface L_g is traveling in the direction $(\pi - \theta_0, \phi_0)$. For a rough surface L_g is also large for directions close to this. In the case of ocean color sensors, this term is minimized by providing the instrument with the capability of tilting the scan plane away from the above direction. Because of this we ignore L_g.*

The diffuse transmittance t can be estimated by using the approximation $t_a \approx 1$. This is possible because the aerosol is strongly forward scattering, so F_a is near unity, and even for mildly absorbing aerosols ω_a is usually greater than about 0.85. Thus, the product $\omega_a F_a \gtrsim 0.75$ in

* For a flat ocean, L_g is orders of magnitude larger than the other radiances in Eq. (25). For a rough ocean it is smaller, but at its maximum could still be one or two orders of magnitude larger than the other terms in the equation. Thus, the region of large L_g must be *avoided*: it cannot be estimated with sufficient accuracy to utilize imagery acquired in the sun glint region.

Eq. (24) and $t_a \approx 1$ as long as τ_a is not too large. (Recall that the assumption that the atmosphere is thin still prevails, and this requires $\tau_a \ll 1$.)

The remaining quantity, L_a, cannot be computed because τ_a is a strong function of space and time. Also, even given τ_a, e.g., from surface measurements of $T(\theta_0, \phi_0)$, computation of L_a requires the aerosol phase function which is very difficult to obtain. Thus, this term must be estimated in some way from measurements made at the sensor. A scheme for carrying this out was first proposed by Gordon[32] in the late 1970's. The basic idea is to use the fact that the water-leaving radiance in the red and/or NIR portion of the spectrum is very small compared to the other terms in Eq. (25). Let $\lambda_i < \lambda_j$ be two spectral bands in this region of the spectrum. Then Eq. (25) can be used to estimate L_a, i.e., $L_a = L_t - L_r$, since $L_w = 0$ in this region and the sensor tilt renders $L_g = 0$ in situations where it might be a problem. Given $L_a(\lambda_i)$ and $L_a(\lambda_j)$ we can form

$$\frac{L_a(\lambda_i)}{L_a(\lambda_j)} = \epsilon(\lambda_i, \lambda_j) \frac{F_0'(\lambda_i)}{F_0'(\lambda_j)}, \tag{27}$$

where

$$\epsilon(\lambda_i, \lambda_j) = \frac{\omega_a(\lambda_i)\tau_a(\lambda_i)\Big(P_a(\alpha_+, \lambda_i) + [\rho(\theta) + \rho(\theta_0)]P_a(\alpha_-, \lambda_i)\Big)}{\omega_a(\lambda_j)\tau_a(\lambda_j)\Big(P_a(\alpha_+, \lambda_j) + [\rho(\theta) + \rho(\theta_0)]P_a(\alpha_-, \lambda_j)\Big)}. \tag{28}$$

For a given aerosol *type*, the aerosol optical thickness is proportional to the concentration, so the concentration cancels out of Eq. (28) and $\epsilon(\lambda_i, \lambda_j)$ is independent of the aerosol concentration. Also, for the aerosol models described earlier, ω_a is very nearly independent of λ, so the $\omega_a(\lambda)$ terms should cancel as well. If the aerosol phase function were independent of λ, then the P_a terms would also cancel, yielding

$$\epsilon(\lambda_i, \lambda_j) = \frac{\tau_a(\lambda_i)}{\tau_a(\lambda_j)}, \tag{29}$$

For a given *aerosol type* $\tau_a(\lambda_i)/\tau_a(\lambda_j)$ is a constant, so $\epsilon(\lambda_i, \lambda_j)$ would be *constant* everywhere in an image in which the aerosol type does not change from one position to another. However, Figures 8 and 9 show that P_a is weakly dependent on λ, so Eq. (29) is only an approximation, and we can expect some variations in ϵ over an image even when the aerosol type does not change. Equations (29) and (10) suggest that it is reasonable to assume that ϵ varies with wavelength according to λ^{-n}, i.e.,

$$\epsilon(\lambda_i, \lambda_j) = \left(\frac{\lambda_j}{\lambda_i}\right)^n, \tag{30}$$

where n is *approximately* constant. Using the value of n estimated in this manner, we can extrapolate $\epsilon(\lambda_i, \lambda_j)$ from the red/NIR into the green and blue regions of the spectrum. This then enables the estimation of $\epsilon(\lambda, \lambda_j)$ and from this $L_a(\lambda)$:

$$L_a(\lambda) = \epsilon(\lambda, \lambda_j) \frac{F_0'(\lambda)}{F_0'(\lambda_j)} L_a(\lambda_j). \tag{31}$$

The procedure described above yields $L_w(\lambda)$ given two other wavelengths for which L_w can either be assumed to be zero or has a known value. When we apply it to the CZCS our goal is to determine L_w at 443, 520, and 550 nm in order to estimate the pigment concentration.[27] We note from Figure 16 that for the lower pigment concentration the approximation $L_w(670) \approx 0$ is reasonable in that $L_w(670) \lesssim 1\%$ of $L_t(670)$. However, L_w at the other bands is a significant portion of L_t and is unknown. Thus, there is not enough information to estimate the values of $\epsilon(\lambda, 670)$ required to execute the procedure. One method for obtaining some information about ϵ was developed by Gordon and Clark,[33] who showed that when $C \leq 0.25$ mg/m^3, the *normalized water leaving radiance*, $[L_w]_N$, defined through

$$L_w(\lambda) = [L_w(\lambda)]_N \cos\theta_0 \exp\left[-(\tau_r/2 + \tau_{Oz})/\cos\theta_0\right], \tag{32}$$

was independent of C and has the values 0.498, 0.30, and less than 0.015 mW/cm^2μm Ster for 520, 550, and 670 nm, respectively. In contrast, at 440 nm even for $C \leq 0.25$ mg/m^3, $[L_w]_N$ depends very strongly on the actual value of C. The normalized water-leaving radiance is approximately the radiance that would exit the ocean if the sun were at the zenith and the atmosphere were removed.

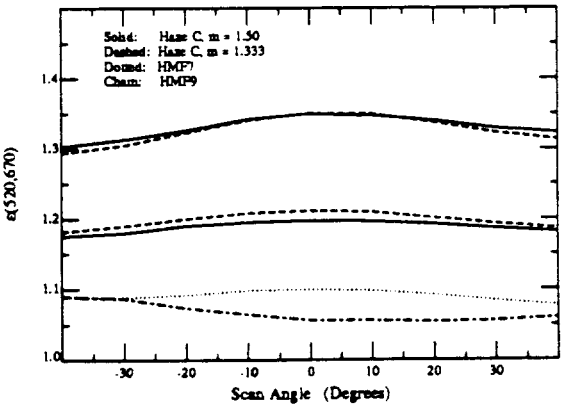

Figure 17. Computed variation of $\epsilon(520, 670)$ across a CZCS scan line for the geometry of Orbit 130 over the Gulf of Mexico (November 2, 1978[3]) using Eq. (28). The upper (lower) solid and dashed curves are for $\nu = 4$ (3).

This clear water radiance concept was utilized by Gordon et al.[24] to process CZCS imagery in the following manner. First, a region of an image for which $C < 0.25$ mg/m^3 was located. Next, the procedure described above was used to determine $\epsilon(520,670)$, $\epsilon(550,670)$, and $\epsilon(670,670)$, and $\epsilon(443,670)$ for this region by extrapolation using Eq. (30). Finally, these values determined for the ϵ parameters were used throughout the entire image.

There are, however, several serious difficulties with this procedure. First, there may be no "clear water" in the image of interest. Second, the aerosol type may vary over the image in which case the ϵ's are expected to depend strongly on position.[34,35] Third, even if the aerosol type remains constant, our models (Figures 8 and 9) show that the aerosol phase function depends weakly on wavelength which implies that the ϵ's will depend on position in the image even if all of the assumptions inherent in the single scattering approximation are valid (Figure 17).[36] Forth, the single scattering approximation is not sufficiently accurate. The necessity of clear water in a scene will be circumvented in future sensors by virtue of additional spectral bands with $\lambda > 700$ nm (Figure 16); however, for CZCS it must be faced head on. The most promising approach is that described for Case 1 waters by Morel and co-workers[34,35] based on earlier ideas of Smith and Wilson[37] (See also, Gordon et al.[25]). In these waters $[L_w]_N$ for a given wavelength is modeled as a function of C. Thus, L_w at each wavelength can be written in terms of C, i.e., ignoring L_g in Eq. (25),

$$L_t(\lambda) = L_r(\lambda) + L_a(\lambda) + tL_w(\lambda, C).$$

Then using Eqs. (30) and (31), we have

$$tL_w(\lambda, C) = L_t(\lambda) - L_r(\lambda) - \left(\frac{\lambda}{\lambda_4}\right)^n \frac{F_0'(\lambda)}{F_0'(\lambda_4)}\left[L_t(\lambda_4) - L_r(\lambda_4) - tL_w(\lambda_4, C)\right], \qquad (33)$$

where $\lambda = \lambda_1$, λ_2, or λ_3. Given $L_w(\lambda, C)$, this equation can be solved for three values of n corresponding to λ_1, λ_2, and λ_3. These are averaged to obtain a single value. An iterative procedure is used to find $L_w(\lambda, C)$ and n as follows:

(1) start by setting $L_w(\lambda_4, C)$ and n to zero and compute $L_w(\lambda, C) \equiv L_w^{(0)}(\lambda, C)$ using Eq. (33);

(2) use the ratio $r_{1,3}$ or $r_{2,3}$ to estimate C;

(3) use the $[L_w]_N$ model for Case 1 waters to estimate $L_w(\lambda, C) \equiv L_w^{(1)}(\lambda, C)$;

(4) use $L_w^{(1)}(\lambda, C)$; in Eq. (33) to estimate a mean $n \equiv n^{(1)}$;

(5) use $n^{(1)}$ in Eq. (33) to estimate $L_w(\lambda, C) \equiv L_w^{(2)}(\lambda, C)$; and

(6) repeat steps (2) through (5) until $n^{(k)}$ and $L_w^{(k)}(\lambda, C)$ converge.

In this manner we arrive at values of C and $L_w(\lambda, C)$ which are consistent with the model for Case 1 waters. Schematically, this procedure is represented by

$$\cdots L_w^{(k)}(\lambda, C) \overset{\text{Eq. (33)}}{\rightarrow} n^{(k)} \overset{\text{Eq. (33)}}{\rightarrow} L_w^{(k+1)}(\lambda, C) \overset{r_{1,3}}{\rightarrow} C \overset{\text{Model}}{\rightarrow} L_w^{(k+2)}(\lambda, C) \overset{\text{Eq. (33)}}{\rightarrow} n^{(k+2)} \cdots,$$

where "Model" refers to the radiance model for Case 1 waters. The virtues of this procedure are (1) that the maximum value of C can be quite large, i.e., 1.5-2.0 mg/m^3, so the clear water requirement can be relaxed, and (2) that the procedure can be applied to images on a pixel-by-pixel basis so the variability of ϵ is irrelevant. However, it must be recalled that the procedure is based on Eq. (30) which is an approximation. Direct comparison between ship-measured and CZCS-derived pigment concentrations can determine the efficacy of this assumption, but only in a very indirect manner. Also, the procedure requires a radiance model of Case 1 waters which is probably *not* representative of *all* Case 1 situations. Case 2 waters, i.e., waters for which other constituents such as dissolved organic material from river runoff or resuspended sediments can influence the optical properties of the medium, must of course be excluded from such a procedure. With these caveats, the only remaining criticism of the atmospheric correction is the forth — that the single scattering approximation is not accurate enough. However, we have made other assumptions that also require examination, e.g., that the sea surface is flat, that a mean O_3 concentration is sufficient, etc. We examine these in the next section.

Second Order Processes

Examination of the influence of the higher order processes on the basic correction algorithm (Eqs. (22) – (31)) have been under way since the mid 1980's. Topics that have been addressed include, the influence of multiple scattering on the basic algorithm,[38,39] the error incurred by

ignoring multiple scattering and polarization in the computation of L_r,[31] the impact of high-altitude volcanically-generated aerosols, e.g., from El Chichón, on the algorithm,[40] the error incurred by ignoring the spatial-temporal variation in the surface atmospheric pressure,[41] and the impact of the assumption that the sea surface is flat.[42,43] We now discuss these individually.

Multiple Scattering

The influence of multiple scattering on the basic CZCS correction algorithm was studied by Deschamps et al.[38] and Gordon and Castaño.[39] In both studies a realistic model of the atmosphere was employed and L_t was derived from radiative transfer equation including all orders of multiple scattering. Deschamps et al. investigated the validity of the equation $L_t = L_r + L_a$ for a model with the sea surface absent. This is analogous to examining the validity of Eq. (25). They computed L_r and L_a separately, i.e., L_r for the case of no aerosols and L_a for the case with no air molecules, and exactly. They concluded that this approximation is in error by an amount that is only slightly above the limit of detectability with CZCS, but will have to be dealt with in future, more sensitive, instruments. Gordon and Castaño included the effects of a flat Fresnel-reflecting sea surface in their computations of L_t. They derived values for L_r which included multiple scattering, and then applied the CZCS algorithm, Eqs. (25), (27), (30) and (31), to a situation in which L_w was known at λ_2, λ_3, and λ_4, and derived $L_w(\lambda_1)$. Computations were carried out for several CZCS orbital geometries. As in the Deschamps et al. study, errors in the derived $L_w(\lambda_1)$ were detected, and explained by an interaction between Rayleigh and aerosol scattering, i.e., by photons scattering from *both* molecules and aerosols. It was found that the simple procedure of reducing the value of $\epsilon(\lambda_1, \lambda_4)$, found from extrapolation using Eq. (30), by 5%, usually reduced the error in $L_w(\lambda_1)$ to 1-2 CZCS digital counts. This procedure was also tested by Gordon and Castaño[40] for situations with a high-altitude aerosol, e.g., produced by the volcano El Chichón in 1982. They showed that the presence of this aerosol should not degrade the atmospheric correction. The message from these studies, however, is clear: the standard CZCS correction algorithm will not be sufficiently accurate to utilize fully the more sensitive instruments proposed for future missions.

Multiple Scattering and Polarization Effects on L_r

Thus far the polarization properties of the light have been ignored; however, a correct treatment of radiative transfer requires that polarization be considered. Kattawar, Plass, and Hitzfelder[44] have shown that ignoring the polarization properties of the light can result in significant errors in the

radiance reflected from a Rayleigh scattering atmosphere. Thus, even when the multiple scattering effects discussed in the previous section are included in the algorithm, if L_r is incorrectly computed by virtue of ignoring polarization, the resulting L_w may still contain significant errors.

When the polarization state of the light is included, the radiance L in the radiative transfer equation is replaced by a vector $\boldsymbol{I}$, and the transport equation becomes[21]

$$\cos\theta \frac{d\boldsymbol{I}(\tau;\theta,\phi)}{d\tau} = -\boldsymbol{I}(\tau;\theta,\phi) + \omega_0 \int_0^{\pi} d\theta' \int_0^{2\pi} d\phi' \sin\theta' \boldsymbol{Z}(\tau;\theta',\phi' \rightarrow \theta,\phi)\boldsymbol{I}(\tau;\theta',\phi'). \qquad (34)$$

The phase function, $p(\tau;\theta',\phi' \rightarrow \theta,\phi)$, in the scalar case (Eq. (13)) is replaced by a 4×4 phase matrix $\boldsymbol{Z}(\tau;\theta',\phi' \rightarrow \theta,\phi)$ in the vector theory. Hansen and Travis[10] show in detail how $\boldsymbol{Z}$ can be derived using Mie theory given the properties of the scattering particles or molecules. The scalar phase function is actually included in $\boldsymbol{Z}$, i.e.,

$$p(\tau;\theta',\phi' \rightarrow \theta,\phi) = Z_{11}(\tau;\theta',\phi' \rightarrow \theta,\phi).$$

The Stokes vector[13,18,21,45] $\boldsymbol{I}$ can be written

$$\boldsymbol{I} = \begin{pmatrix} I \\ Q \\ U \\ V \end{pmatrix},$$

where I is the radiance measured by an instrument that is *insensitive* to the polarization state of the light (denoted by L in the *scalar* theory). The polarization characteristics of the light are determined by the other components of $\boldsymbol{I}$, for example, the degree of polarization of the radiation is

$$P = \frac{\sqrt{Q^2 + U^2 + V^2}}{I},$$

where $0 \leq P \leq 1$. $P = 0$ corresponds to completely unpolarized light and $P = 1$ completely polarized light. Light with an intermediate value of P is partially polarized. When $V = 0$ and $P \neq 0$ the light is said to be linearly polarized, otherwise it is elliptically polarized.

A complete multiple scattering solution of Eq. (34) can be obtained by the method of successive orders of scattering in a manner similar to Eq. (13). Gordon, Brown, and Evans[31] have carried out such a solution for unpolarized sunlight falling on a Rayleigh scattering atmosphere bounded below by a flat Fresnel-reflecting ocean. Their computations showed that the single scattering solution for L_r, i.e., Eq. (22) with $x = r$, was typically about 3-5% too low over the center 80% of the

CZCS scan for geometries with $\theta_0 \lesssim 50°$. An example of this is given in Figure 18 which provides the % difference between the exact Rayleigh contribution, L_r(Exact), for CZCS Band 1, computed by considering all orders of multiple scattering including polarization, i.e., solving Eq. (34), and that computed using approximate methods, L_r(Approx.). The geometry is that of Orbit 3226 over the Middle Atlantic Bight.[24,31] For the solid line L_r(Approx.) is computed using single scattering, i.e., Eq. (22), while for the dashed line it is computed by accounting for all orders of multiple scattering but *neglecting* polarization, i.e., solving Eq. (13). The small variability of the error in the single-scattering L_r with scan and sun angle explains its success: the error was effectively removed by adjusting the sensor calibration near the start of the mission.[24,31] For large values of

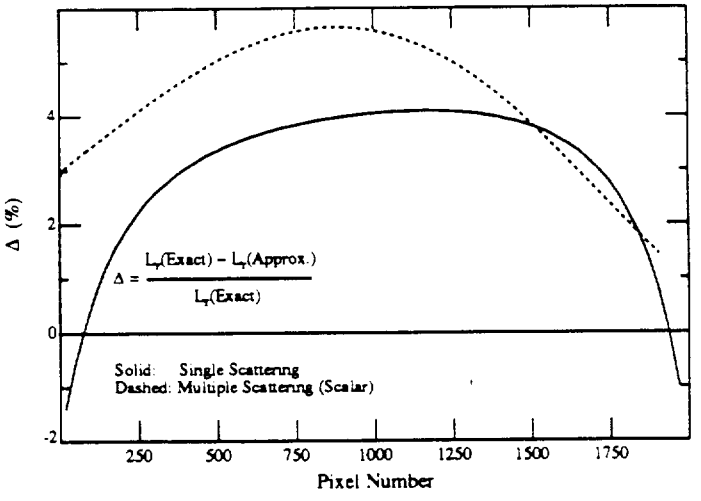

Figure 18. Percent difference between the exact Rayleigh contribution, L_r(Exact), and that computed using approximate methods L_r(Approx.), for CZCS Band 1.

θ_0, the single-scattering L_r becomes larger and the error can reach as much as 15% for $\theta_0 \approx 70°$. However, when the solution to Eq. (34) is used in the computation of L_w, atmospheric corrections have been demonstrated for $\theta_0 \lesssim 70°$. So far I have compared only single scattering L_r with the exact value computed including all multiple scattering and polarization effects. It is natural to ask if it is possible to ignore polarization and find L_r by solving the scalar transport equation, Eq. (13). Gordon, Brown, and Evans[31] also investigated this question and found that in some cases, calculating L_r by including multiple scattering but ignoring polarization actually produced *larger* errors than the single scattering approximation (Figure 18). Tables of L_r including multiple

scattering and polarization are available and are being used at many locations.* The accuracy in the computation of L_r for CZCS is now limited by the accuracy with which the O_3 concentration and surface atmospheric pressure are known.

Ozone and Surface Pressure Variations

The surface atmospheric pressure varies as weather systems move across the globe. Similar (noncorrelated) variations are observed in the total Ozone concentration as stratospheric "weather" systems move over the globe. In fact, the Ozone concentration over a given location can vary by more than 100 DU over a period of a few days.[47] This is an enormous variation considering the mean O_3 concentration is only about 350 DU. The surface pressure variation causes variations in τ_r (Eq. (9)) which in turn cause variations in L_r. From Eqs. (9) and (22) we see that if $P_0 \rightarrow P_0 + \Delta P$, then $L_r \rightarrow L_r + (\Delta L_r)_P$, where

$$\frac{(\Delta L_r)_P}{L_r} = \frac{\Delta P}{P_0}.$$

For a variation of 15 mb around $P_0 = 1013$ mb, this gives $(\Delta L_r)_P / L_r = \pm 1.5\%$. The O_3 variation influences L_r through its influence on F_0' (Eqs. (22) and (23)). It is easy to see that if $\tau_{oz} \rightarrow \tau_{oz} + \Delta\tau_{oz}$, then $L_r \rightarrow L_r + (\Delta L_r)_O$, where

$$\frac{(\Delta L_r)_O}{L_r} = -\Delta\tau_{oz}\left(\frac{1}{\cos\theta_0} - \frac{1}{\cos\theta}\right),$$

or

$$\frac{|(\Delta L_r)_O|}{L_r} = |\Delta\tau_{oz}|\left(\frac{1}{\cos\theta_0} - \frac{1}{\cos\theta}\right) > 2\,|\Delta\tau_{oz}|.$$

Now, $\tau_{oz} = a^*_{O_z} C_{Oz}$, where $a^*_{O_z}$ is the *specific* O_3 absorption coefficient and C_{Oz} is the O_3 in DU. At 550 nm, Figure 3 suggests that $\tau_{oz} \approx 0.03$ for $C_{Oz} = 350$ DU. Thus, for a ± 50 DU variation around 350 DU we can expect $|(\Delta L_r)_O| / L_r > 0.008$ or $\sim$1%. Although these variations in L_r are small, they can make a significant impact on the retrieved pigment concentration[41] because they vary strongly with wavelength. They lead to errors in L_w which also vary strongly with wavelength.

* Eckstein and Simpson[46] have suggested that use of these tables can result in very large errors in atmospheric correction due to large differences ($\gtrsim$ 20%) they claim to observe between the single scattering and the multiple scattering values of L_r. However, this *incorrect* conclusion is the result of their *misinterpretation* of the geometry employed for the multiple scattering results in Gordon, Brown, and Evans.[31] In most cases, unless $\theta_0 \gtrsim 65°$, the differences between the exact and single scattering values of L_r are similar to that shown in Figure 18.

For example, in the ratio r_{13}, O_3 variations principally influence $L_w(\lambda_3)$, while variations in P principally influence $L_w(\lambda_1)$. The magnitude of the errors in the pigment concentration resulting from P and O_3 variations has been thoroughly discussed by André and Morel.[41] The only way to correctly address these problems is to have fields of P and O_3 available for inclusion in the data processing. In the case of CZCS the O_3 concentration is available from other sensors on NIMBUS-7 and they have been included in the processing stream; however, in the case of variations in P there are no data fields simultaneous with CZCS and thus far these variations have been ignored. In the case of future instruments, e.g., SeaWiFS, OCTS, and MODIS, pressure fields derived from numerical weather models will be used to incorporate estimates of P.

Rough Surface Effects

In all of the computations described so far, it has been assumed that the sea surface is flat. Neglecting direct sun glitter L_g, in the application of the algorithm, this assumption is utilized *only* in the computation of L_r. The basic effect of the surface roughness is to change the boundary condition at the lower boundary of the atmosphere (the sea surface). In contrast to the flat ocean case (Eq. (15)), reflection from the rough surface is described by a bi-directional reflectance distribution function (BRDF), and is given by

$$L(z_1, \theta_r, \phi_r) = \int_{2\pi} r(\theta_i, \phi_i \rightarrow \theta_r, \phi_r) L(z_1, \theta_i, \phi_i)\, d\Omega_i, \tag{35}$$

where the 2π on the integral indicates that the integration is to be taken over 2π Ster of Ω_i. The quantity $r(\theta_i, \phi_i \rightarrow \theta_r, \phi_r)$ specifies the BRDF of the surface. Gordon and Wang[42] carried out multiple scattering computations, including polarization, for a Rayleigh scattering atmosphere assuming that the wind-ruffled sea surface consists of a collection of individual facets obeying the slope statistics derived by Cox and Munk.[48] For simplicity, the surface slope distribution was assumed to be independent of the wind direction. They found that, in the case of CZCS, the effect of surface roughness was usually below the detectable range for wind speeds up to 16.9 m/s when the sun angle was 40°; however, for $\theta_0 = 60°$ the difference between the flat and rough surface, although usually small, could become as large as three CZCS digital counts for large scan angles at 670 nm. They showed that the maximum error in assuming the ocean was flat in the computation of L_r was about the same order of magnitude as that which would arise from a ± 15 mb variation in P or a ± 50 DU variation in the O_3 concentration; however, the overall effect is smaller than that of variations in O_3 and P because the error is more spectrally neutral. By simulating the entire

correction process,[43] they concluded that little would be gained by including surface roughness effects in routine CZCS processing, but demonstrated that such information may be required for more sensitive instruments.

Correction of Future Sensors

The next generation ocean color sensors, such as SeaWiFS[49] and MODIS[50,51] will have a radiometric sensitivity that is superior to CZCS. Several effects thus far ignored in the CZCS processing algorithms, but which must be included in order that the improved radiometric sensitivities can be fully utilized are listed below.

- The interaction between Rayleigh and aerosol scattering.
- The curvature of the earth.
- The large ϵ extrapolation required.
- The presence of whitecaps on the sea surface.
- The residual polarization sensitivity of the sensor.

These will now be discussed individually.

Interaction Between Rayleigh and Aerosol Scattering

The basic equation of the CZCS atmospheric correction algorithm is Eq. (25), which was derived from the single scattering approximation. Although L_r is computed using the multiple scattering method (including polarization) described earlier, an error still remains. Basically, even if L_r and L_a both include all orders of multiple scattering, i.e., L_r is computed using a multiple scattering code with $\tau_a = 0$ and L_a computed with $\tau_r = 0$, Eq. (25) still does not allow for the possibility that photons can scatter from *both* aerosols and air molecules. This is called the Rayleigh-aerosol interaction, and was first described quantitatively by Deschampes et al.[38] To increase the accuracy of the CZCS algorithm to deal with the more sensitive instruments, it is necessary to modify Eq. (25) to explicitly include the interaction, i.e.,

$$L_t(\lambda) = L_r(\lambda) + L_a(\lambda) + L_{ra}(\lambda) + L_g(\lambda) + tL_w(\lambda), \tag{36}$$

and to provide a way of computing the interaction, L_{ra}.

Using the ideas of Gordon and Castaño,[39] Wang[52]and Wang and Gordon[53] have developed a technique for including the Rayleigh-aerosol interaction into the formalism without directly calculating L_{ra}. Briefly, they found through a large number of radiative transfer simulations that a linear relationship exists between $L_a + L_{ra}$ and the single-scattered aerosol radiance, i.e.,

$$L_a(\lambda) + L_{ra}(\lambda) = I(\lambda) + S(\lambda)L_{as}(\lambda), \tag{37}$$

where L_{as} is given by Eq. (22) with $x = a$. These simulations included several aerosol models (phase functions), several wind speeds (0 to 16.9 m/s), and aerosol optical thicknesses over the range $\tau_a = 0$ to 0.6. The results showed that, in geometries similar to those employed in ocean color sensing, the values of the "intercept" I and the "slope" S depend strongly on the geometry but very weakly on the aerosol model and the wind speed. Thus, I and S determined from these model computations should be applicable for use in atmospheric correction. The plan is to use Eq. (37) to estimate L_{as} in spectral regions in which $L_w \approx 0$, e.g., 750 and 865 nm for SeaWiFS and most other proposed ocean color sensors, and then to use L_{as} in place of L_a in Eqs. (27) through (31). This procedure would provide L_{as} in the blue and green regions of the spectrum from L_{as} in the red and NIR. Equation (37) would then yield $L_a(\lambda) + L_{ra}(\lambda)$ at the short wavelengths, from which

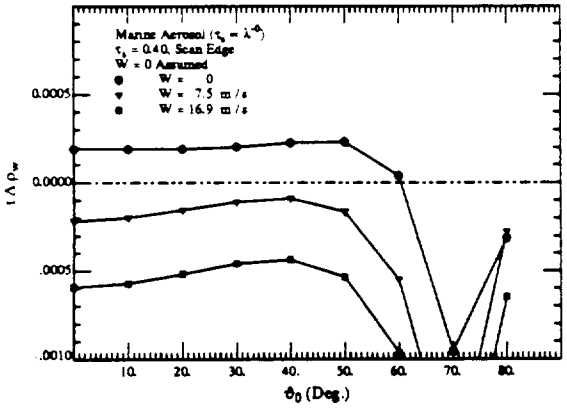

Figure 19. Simulated error in the new atmospheric correction algorithm at the CZCS scan edge as a function of θ_0. The wind speed has been assumed to be unknown and $W = 0$ used in the computation of L_r.

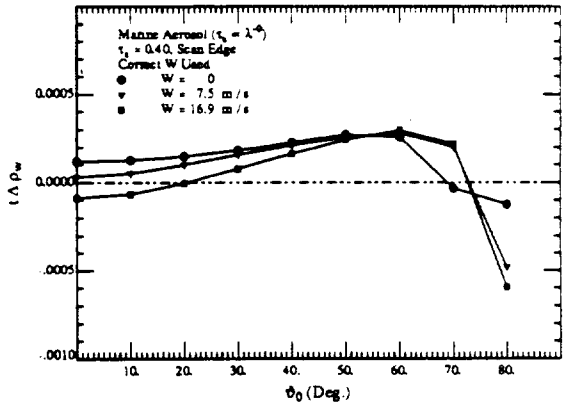

Figure 20. Simulated error in the new atmospheric correction algorithm at the CZCS scan edge as a function of θ_0. The wind speed has been assumed to be known and the correct value is used in the computation of L_r, I, and S.

Eq. (36) can be solved for L_w in the absence of L_g. Since I and S depend weakly on the surface roughness, knowledge of the wind speed improves the accuracy of the algorithm.

This scheme has been tested for an ocean color instrument, with the CZCS band set, observing clear water, i.e., it is assumed that $L_w(\lambda)$ is given for λ_2, λ_3, and λ_4 and that we want to retrieve

$L_w(\lambda_1)$. An example of the resulting error for a relatively turbid atmosphere is provided in Figure 19 in which $\Delta\rho_w = \pi\Delta L_w/F_0\cos\theta_0$ is the error in the retrieved water-leaving *reflectance*. The aerosol is assumed to be nonabsorbing, to have a scattering coefficient that is independent of λ, and to have a scattering phase function that is approximately the average of HMF7 and HMF9. The wind speed W has been assumed to be unknown, so $W = 0$ has been used in the computation of L_r. For reference, 1 DC at Gain 1 (see Appendix) for CZCS would correspond to a reflectance of 0.00076 at $\theta_0 = 0$ and 0.00153 at $\theta_0 = 60°$. Thus, in this example, the error in $L_w(\lambda_1)$ would usually be less than 1 CZCS DC even though the surface roughness is ignored. Figure 20 shows the improvement that results when the correct wind speed is used in the algorithm. Wang and Gordon's[53] analysis suggests that this procedure can provide an atmospheric correction that is nearly an order of magnitude more accurate than the standard CZCS algorithm.

The Large ϵ Extrapolation

Following the scheme proposed above for the new ocean color sensors, the quantities determined from the NIR bands are $\epsilon(750, 865)$ and $\epsilon(865, 865)$ in Eq. (28). These must be extrapolated into the visible to obtain $\epsilon(\lambda, 865)$, where λ can be as small as 410 nm. Thus, it will be necessary to understand the manner in which ϵ values determined in the NIR relate to those in the visible. This question is being studied now, within the limits imposed by the nonspherical nature of the aerosol, using Mie theory models of aerosol scattering.

The Effect of Earth Curvature

All atmospheric corrections algorithms developed thus far ignore the curvature of the earth, i.e., the plane parallel atmosphere (PPA) approximation has always been used in the radiative transfer simulations for ocean remote sensing. However, at the level of accuracy required to use the full sensitivity of new instruments, it may be necessary to take the curvature of the earth into account,[31] particularly at large sun angles. For example, Figure 21 shows the error in L_r caused by the assumption of a plane parallel atmosphere at the scan center and the scan edge of a sensor like SeaWiFS (Gordon and Ding, unpublished). For $\theta_0 \lesssim 60°$ the error is $< 1\%$ and can be ignored for CZCS and possibly SeaWiFS; however, for larger θ_0, e.g., high latitudes, the error becomes excessive. Computations by Adams and Kattawar,[54] suggest that nearly all of the difference between the PPA approximation and the true spherical shell atmosphere (SSA) is in the first scattering, i.e., the fraction of the radiance due to multiple scattering is approximately the

same for the PPA and SSA. An effort is now under way at the University of Miami to use this to

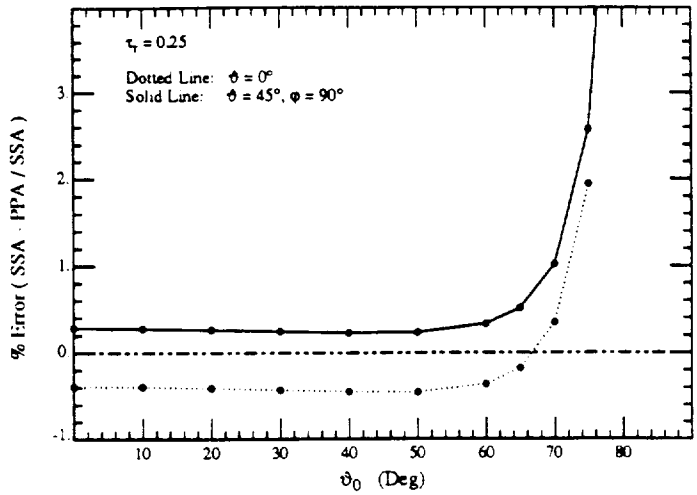

Figure 21. Error in L_r computed under the plane parallel assumption for the atmosphere.

provide a first order correction for the effects of earth curvature.

Whitecaps

Gordon and Jacobs[55] have presented computations suggesting that sea foam (whitecaps) could significantly increase the flux leaving the top of the atmosphere over the oceans. This added radiance, must be considered in the radiance budget at the sensor. The effect of whitecaps can be estimated[56] by combining Koepke's[57] determinations of the surface reflectance *increase* due to whitecaps as a function of the wind speed, with extrapolations into the blue green region of the spectrum of laboratory measurements of the foam reflectance spectrum in the red and NIR made by Whitlock *et al.*[58] The result is provided in Figure 22. The figure gives the contribution of whitecaps to the radiance at the top of the atmosphere for the four CZCS bands. The radiance is in CZCS Gain 1 digital counts (See Appendix). It is seen that even wind speeds below *mean* values, which only rarely reach 7–8 m/s,[59–61] whitecaps increase the radiance in the CZCS red band by a measurable amount. This increase is ignored in CZCS processing. With higher radiometric sensitivity and with spectral bands in the NIR, whitecaps will influence L_t for new sensors at even lower wind speeds. The increased radiance will be interpreted as aerosol by the atmospheric correction algorithm yielding incorrect water-leaving radiances. If ignored, the expected improvement over CZCS due to the presence of the NIR "atmospheric correction" bands will be degraded. It is possible to

develop a whitecap removal algorithm based on our present knowledge, i.e., given the wind speed, the whitecap reflectance could be estimated in a manner similar to that used to prepare Figure 22 and removed from L_t *before* atmospheric correction. However, the present analysis ignores the sea surface temperature, which Bortkovskii[62] reports can significantly influence the foam coverage of the sea surface. Thus, it is believed that for an accurate assessment and removal of whitecap

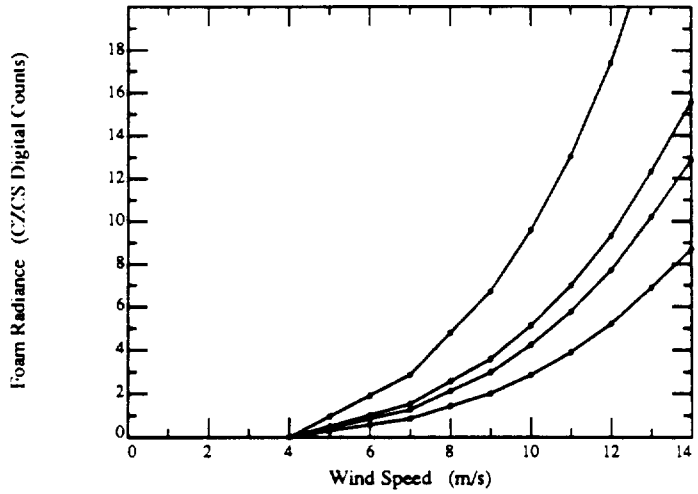

Figure 22. Increase in L_t in CZCS digital counts resulting from whitecaps on the sea surface. Curves from bottom to top correspond to CZCS Bands 1-4, respectively.

effects, more experimental measurements are needed. The issues that must be addressed to deal with whitecaps are as follows: first, the relationship between whitecap coverage, wind speed, and sea surface temperature is not well understood and needs to be; next, the spectral reflectance of individual whitecaps has never been measured in the field (nor in the laboratory in the blue and green regions of the spectrum) and should be; and finally, the increase in surface reflectance due to whitecaps has not been measured directly, it has been deduced from the individual whitecap reflectance and the fraction of the surface covered, e.g., Figure 22. For the purposes of remote sensing, field measurements of the actual increase in the average reflectance, over areas with sizes of the order of a km, as a function of variables that can be measured from space or deduced from numerical models, e.g., wind speed and sea surface temperature, would provide the most direct way of developing the necessary removal algorithm.

Residual Instrument Polarization Sensitivity

The typical specification — that the polarization sensitivity of ocean color sensors should be less than 2% — is based on the requirement that the unknown polarization of L_t induced by the aerosols can be corrected using aerosol models.[63] This implies the processing will still be required to remove the the residual polarization effects. We have developed a formalism[63]which provides the framework for such processing.

Summary

In this paper I have tried to provide a more or less self-contained discussion on the optical properties of the atmosphere and radiative transfer theory to provide the reader with an understanding of atmospheric correction of satellite ocean color remote sensing data. The absorption properties of the optically important gases (H_2O, O_2, and O_3) in the atmosphere have been presented in the form of spectral transmittance curves. The scattering properties of the aerosol have been described with examples taken from Mie scattering theory applied to aerosol models. The development of the CZCS algorithm has been described in detail starting from the single scattering solution of the radiative transfer theory. A critical evaluation of the model is then carried out and efforts to circumvent the difficulties specific to the CZCS band set are presented. Processes ignored in the original algorithm but included in later versions, e.g., multiple scattering, polarization, and variations in the O_3 concentration and the surface atmospheric pressure, are briefly examined. Finally, the question of atmospheric correction of future, more sensitive, ocean color sensors, such as SeaWiFS, is considered. An improved correction algorithm is proposed and the remaining problems, along with suggested approaches for solving them, are described.

Appendix: CZCS Radiometry

The CZCS data was digitized to 8-bits on board the satellite and relayed to the ground in digital form. The sensor sensitivity was adjustable to four levels (Gains). The approximate radiance increment corresponding to a change in the output of one digital count (DC) is presented in Table

A1.[64,65] Under ideal operation the sensitivity would vary along the orbit to account for the decrease

Table A1: Radiance (DC) in mW/cm^2 μm Ster corresponding to one digital count for the four CZCS sensitivities.

Band	λ	DC			
	(nm)	Gain 1	Gain 2	Gain 3	Gain 4
1	433–453	0.045	0.036	0.030	0.021
2	510–530	0.031	0.025	0.020	0.015
3	540–560	0.025	0.020	0.016	0.012
4	660–680	0.011	0.0090	0.0074	0.0053

of incident solar irradiance with latitude away from the solar equator. In practice, most data were acquired at Gains 1 and 2. At typical signal levels the signal-to-noise ratio is above 150 for all bands with the exception of Band 4, for which the measured value was 118.[2] The data provided in the table was applicable at launch (October 1978). The sensitivity of the CZCS degraded in orbit from the values presented above. This degradation has been described by Gordon et al.,[66] Mueller,[67] Hovis et al.,[68] and Gordon and Evans.[69] It amounts to as much as a 40% drop in sensitivity during the eight years of operation. The author believes that this variation in sensitivity with time on both short and long time scales accounts for much of the difficulties and inconsistencies encountered with CZCS data. For SeaWiFS, the long-term and short-term variability of the sensitivity will be accurately monitored by viewing the moon and an internal reflectance standard, respectively.

The CZCS was designed to be insensitive to the polarization state of the incident radiance, i.e., if the incident radiance was 100% linearly polarized and the direction of polarization was rotated through 180°, the output was supposed to vary less than about 2%.

References

[1] G. L. Clarke, G. C. Ewing and C. J. Lorenzen, "Spectra of Backscattered Light from the Sea Obtained From Aircraft as a Measurement of Chlorophyll Concentration," Science **167**, 1119–1121 (1970).

[2] W. A. Hovis, D. K. Clark, F. Anderson, R. W. Austin, W. H. Wilson, E. T. Baker, D. Ball, H. R. Gordon, J. L. Mueller, S. Y. E. Sayed, B. Strum, R. C. Wrigley and C. S. Yentsch, "Nimbus 7 coastal zone color scanner: system description and initial imagery," Science **210**, 60–63 (1980).

[3] H. R. Gordon, D. K. Clark, J. L. Mueller and W. A. Hovis, "Phytoplankton pigments derived from the Nimbus–7 CZCS: initial comparisons with surface measurements," Science **210**, 63–66 (1980).

[4] T. Platt and S. Sathyendranath, "Oceanic Primary Production: Estimation by Remote Sensing at Local and Regional Scales," Science **241**, 1613–1620 (1988).

[5] A. Morel and J. -M. André, "Pigment Distribution and Primary Production in the Western Mediterranean as Derived and Modeled From Coastal Zone Color Scanner Observations," Jour. Geophys. Res. **96C**, 12,685–12,698 (1991).

[6] R. W. Preisendorfer, "Application of Radiative Transfer Theory to Light Measurements in the Sea," Union Géodésique et Géophysique Internationale **10**, 11–30 (1961).

[7] R. W. Preisendorfer, "*Hydrologic Optics V. 1: Introduction*," 1976, (NTIS PB–259 793/8ST). Natl. Tech. Inform. Serv., Springfield.

[8] F. X. Kneizys, E. P. Shettle, L. W. Abreu, J. H. Chetwynd, G. P. Anderson, W. O. Gallery, J. E. A. Selby and S. A. Clough, *Users Guide to LOWTRAN 7* (Air Force Geophysics Laboratory, AFGL-TR-88-0177, 1988).

[9] NASA, *U.S. Standard Atmosphere Supplements* (1976), U.S. Government Printing Office, Washington, D.C..

[10] J. E. Hansen and L. D. Travis, "Light Scattering in Planetary Atmospheres," Space Science Reviews **16**, 527–610 (1974).

[11] G. Mie, "Beiträge zur Optik trüber Medien, speziell kollidalen Metall-lösungen," Ann. Phys. **25**, 377–445 (1908).

[12] C. F. Bohren and D. R. Huffman, *Absorption and Scattering of Light by Small Particles* (Wiley, New York, 1983), 530 pp.

[13] H. C. van de Hulst, *Light Scattering by Small Particles* (Wiley, New York, 1957), 470 pp.

[14] D. Deirmendjian, *Electromagnetic Scattering on Spherical Polydispersions* (Elsevier, New York, NY, 1969), 290 pp.

[15] H. Quenzel and M. Kastner, "Optical properties of the atmosphere: calculated variability and application to satellite remote sensing of phytoplankton," Applied Optics **19**, 1338–1344 (1980).

[16] L. Elterman, *UV, Visible, and IR Attenuation for Altitudes to 50 km, 1968* (AFCRL, Bedford, MA, Report AFCRL-68-0153, April 1968).

[17] K. M. Case, "Transfer Problems and the Reciprocity Principle," Rev. Mod. Phys. **29**, 651–663 (1957).

[18] H. C. van de Hulst, *Multiple Light Scattering* (Academic Press, New York, 1980), 739 pp.

[19] H. R. Gordon, "Modeling and Simulating Radiative Transfer in the Ocean," in *Ocean Optics*, edited by R. W. Spinrad, K. L. Carder and M. J. Perry (Oxford, 1992) , Submitted.

[20] H. Neckel and D. Labs, "The Solar Radiation Between 3300 and 12500 Å," Solar Physics **90**, 205–258 (1984).

[21] S. Chandrasekhar, *Radiative Transfer* (Oxford University Press, Oxford, 1950), 393 pp.

[22] D. Tanre, M. Herman, P. Y. Deschamps and A. de Leffe, "Atmospheric modeling for space measurements of ground reflectances, including bidirectional properties," Applied Optics **18**, 3587–3594 (1979).

[23] P. Y. Deschamps, M. Herman, J. Lenoble, D. Tanre and M. Viollier, "Atmospheric Effects in Remote Sensing of Ground and Ocean Reflectances," in *Remote Sensing of Oceans and Atmospheres*, edited by A. Deepak (Academic Press, New York, NY, 1981) p. 115–147.

[24] H. R. Gordon, D. K. Clark, J. W. Brown, O. B. Brown, R. H. Evans and W. W. Broenkow, "Phytoplankton pigment concentrations in the Middle Atlantic Bight: comparison between ship determinations and Coastal Zone Color Scanner estimates," Applied Optics **22**, 20–36 (1983).

[25] H. R. Gordon, O. B. Brown, R. H. Evans, J. W. Brown, R. C. Smith, K. S. Baker and D. K. Clark, "A Semi-Analytic Radiance Model of Ocean Color," Jour. Geophys. Res. **93D**, 10909–10924 (1988).

[26] A. Morel and L. Prieur, "Analysis of Variations in Ocean Color," Limnology and Oceanography **22**, 709–722 (1977).

[27] H. R. Gordon and A. Y. Morel, *Remote Assessment of Ocean Color for Interpretation of Satellite Visible Imagery: A Review* (Springer-Verlag, New York, 1983), 114 pp.

[28] A. Morel, "Optical Modeling of the Upper Ocean in Relation to Its Biogenous Matter Content (Case I Waters)," Jour. Geophys. Res. **93C**, 10,749–10,768 (1988).

[29] H. R. Gordon and D. K. Clark, "Atmospheric effects in the remote sensing of phytoplankton pigments," Boundary-Layer Meteorology **18**, 299–313 (1980).

[30] D. K. Clark, "Phytoplankton Algorithms for the Nimbus-7 CZCS," in *Oceanography from Space*, edited by J. R. F. Gower (Plenum Press, New York, NY, 1981) p. 227–238.

[31] H. R. Gordon, J. W. Brown and R. H. Evans, "Exact Rayleigh Scattering Calculations for use with the Nimbus-7 Coastal Zone Color Scanner," Applied Optics **27**, 862–871 (1988).

[32] H. R. Gordon, "Removal of Atmospheric Effects from Satellite Imagery of the Oceans," Applied Optics **17**, 1631–1636 (1978).

[33] H. R. Gordon and D. K. Clark, "Clear water radiances for atmospheric correction of coastal zone color scanner imagery," Applied Optics **20**, 4175–4180 (1981).

[34] A. Bricaud and A. Morel, "Atmospheric Corrections and Interpretation of Marine Radiances in CZCS Imagery: Use of a Reflectance Model," Oceanologica Acta **7**, 33–50 (1987).

[35] J. -M. André and A. Morel, "Atmospheric Corrections and Interpretation of Marine Radiances in CZCS Imagery, Revisited," Oceanologica Acta **14**, 3–22 (1991).

[36] H. R. Gordon, *Some Studies of Atmospheric Optical Variability in Relation to CZCS Atmospheric Correction* (NOAA National Environmental Satellite and Data Information Service, Final Report Contract No. NA–79–SAC–00714, February 1984).

[37] R. C. Smith and W. H. Wilson, "Ship and satellite bio-optical research in the California Bight," in *Oceanography from Space*, edited by J. F. R. Gower (Plenum, New York, NY, 1981) , p. 281–294.

[38] P. Y. Deschamps, M. Herman and D. Tanre, "Modeling of the atmospheric effects and its application to the remote sensing of ocean color," Applied Optics **22**, 3751–3758 (1983).

[39] H. R. Gordon and D. J. Castaño, "Aerosol Analysis with the Coastal Zone Color Scanner: A Simple Method for Including Multiple Scattering Effects," Applied Optics **28**, 1320–1326 (1989).

[40] H. R. Gordon and D. J. Castaño, "The Coastal Zone Color Scanner Atmospheric Correction Algorithm: Influence of El Chichón," Applied Optics **27**, 3319–3321 (1988).

[41] J. -M. André and A. Morel, "Simulated Effects of Barometric Pressure and Ozone Content Upon the Estimate of Marine Phytoplankton From Space," Jour. Geophys. Res. **94C**, 1029–1037 (1989).

[42] H. R. Gordon and M. Wang, "Surface Roughness Considerations for Atmospheric Correction of Ocean Color Sensors. 1: The Rayleigh Scattering Component," Applied Optics **31**, 0000–0000 (1992).

[43] H. R. Gordon and M. Wang, "Surface Roughness Considerations for Atmospheric Correction of Ocean Color Sensors. 2: Error in the Retrieved Water-leaving Radiance," Applied Optics **31**, 0000–0000 (1992).

[44] G. W. Kattawar, G. N. Plass and S. J. Hitzfelder, "Multiple scattered radiation emerging from Rayleigh and continental haze layers. 1: Radiance, polarization, and neutral points," Applied Optics **15**, 632–647 (1976).

[45] W. A. Shurcliff, *Polarized Light* (Havard University Press, Cambridge, MA, 1962), 207 pp.

[46] B. A. Eckstein and J. J. Simpson, "Aerosol and Rayleigh Radiance Contributions to Coastal Zone Color Scanner Images," Int. J. Remote Sensing **12**, 135–168 (1991).

[47] P. K. Bhartia, K. F. Klenk, C. K. Wong, D. Gordon and A. J. Fleig, "Comparison of the NIMBUS 7 SBUV/TOMS Total Ozone Data Sets With Dobson and M83 Results," Jour. Geophys. Res. **89D**, 5239–5247 (1984).

[48] C. Cox and W. Munk, "Measurements of the Roughness of the Sea Surface from Photographs of the Sun's Glitter," Jour. Opt. Soc. of Am. **44**, 838–850 (1954).

[49] NASA and the Earth Observations Satellite Company, *System Concept for Wide-Field-of-View Observations of Ocean Phenomena from Space* (August 1987).

[50] NASA, *MODIS (Moderate-Resolution Imaging Spectrometer), Earth Observing System Volume IIb* (1986).

[51] NASA, *Earth Observing System (Eos) Background Information Package, Announcement of Opportunity No. OSSA-1-88* (Announcement of Opportunity No. OSSA-1-88, January 1988).

[52] M. Wang, "*Atmospheric Correction of the Second Generation Ocean Color Sensors*," 1991, Ph.D. Dissertation, University of Miami, Coral Gables FL, 135 pp.

[53] M. Wang and H. R. Gordon, "Atmospheric Correction of Second Generation Ocean Color Sensors: A Preliminary Algorithm," Applied Optics **31**, 0000–0000 (1992).

[54] C. N. Adams and G. W. Kattawar, "Radiative Transfer in Spherical Shell Atmospheres I. Rayleigh Scattering," Icarus **35**, 139–151 (1978).

[55] H. R. Gordon and M. M. Jacobs, "The Albedo of the Ocean-Atmosphere System: Influence of Sea Foam," Applied Optics **16**, 2257–2260 (1977).

[56] H. R. Gordon, "Calibration Requirements and Methodology for Remote Sensors Viewing the Oceans in the Visible," Remote Sensing of Environment **22**, 103–126 (1987).

[57] P. Koepke, "Effective Reflectance of Oceanic Whitecaps," Applied Optics **23**, 1816–1824 (1984).

[58] C. H. Whitlock, D. S. Bartlett and E. A. Gurganus, "Sea Foam Reflectance and Influence on Optimum Wavelength for Remote Sensing of Ocean Aerosols," Geophys. Res. Lett. **7**, 719–722 (1982).

[59] J. S. Malkus, "Large Scale Interactions," in *The Sea*, edited by M. N. Hill (Wiley-Interscience, New York, NY, 1962) p. 88–294.

[60] W. S. von Arx, *An Introduction to Physical Oceanography* (Addison-Wesley, Reading, MA, 1962), 422 pp.

[61] J. Hsiung, "Mean Surface Energy Fluxes Over the Global Ocean," Jour. Geophys. Res. **91C**, 10,585–10,606 (1986).

[62] R. S. Bortkovskii, *Air-Sea Exchange of Heat and Moisture During Storms* (Reidel, Dordrecht, 1987), 194 pp.

[63] H. R. Gordon, "Ocean Color Remote Sensing Systems: Radiometric Requirements," Society of Photo-Optical Instrumentation Engineers, Recent Advances in Sensors, Radiometry, and Data Processing for Remote Sensing **924**, 151–167 (1988).

[64] Ball Aerospace Division, Boulder CO, *Development of the Coastal Zone Color Scanner for Nimbus-7: Volume 1 – Mission Objectives and Instrument Description* (Final Report F78-11, Rev. A NASA Contract NAS5-20900, May 1979).

[65] Ball Aerospace Division, Boulder CO, *Development of the Coastal Zone Color Scanner for Nimbus-7: Volume 2 – Test and Performance Data* (Final Report F78-11, Rev. A NASA Contract NAS5-20900, May 1979).

[66] H. R. Gordon, J. W. Brown, O. B. Brown, R. H. Evans and D. K. Clark, "Nimbus 7 Coastal Zone Color Scanner: reduction of its radiometric sensitivity with time," Applied Optics **22**, 3929–3931 (1983).

[67] J. L. Mueller, "Nimbus-7 CZCS: confirmation of its radiometric sensitivity decay rate through 1982," Applied Optics **24**, 1043–1047 (1985).

[68] W. A. Hovis, J. S. Knoll and G. R. Smith, "Aircraft Measurements for Calibration of an Orbiting Spacecraft Sensor," Applied Optics **24**, 407–410 (1985).

[69] H. R. Gordon and R. H. Evans, "*The CZCS: Algorithms and Characterization*," OCEANS FROM SPACE, Scuola Grande San Giovanni Evangelista, Venice, Italy, May 22–26, 1990.